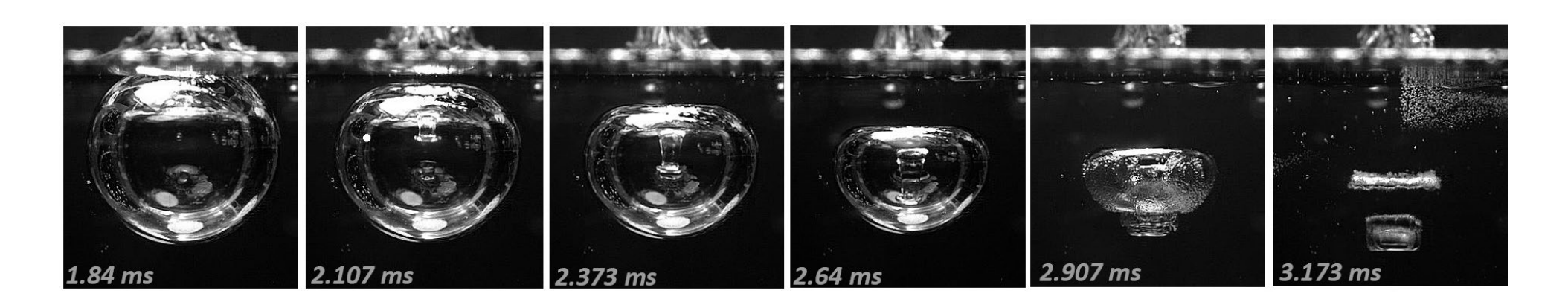
SECTION DE GENIE MECANIQUE 6th & 8th Semester, Fall 2024

CAVITATION AND INTERFACE PHENOMENA

Chapter 3 : Dynamics of non-spherical cavitation bubbles

3.2 : Micro-Jetting



Dr Mohamed FARHAT Assistants: Th. Berger, A. Sache.

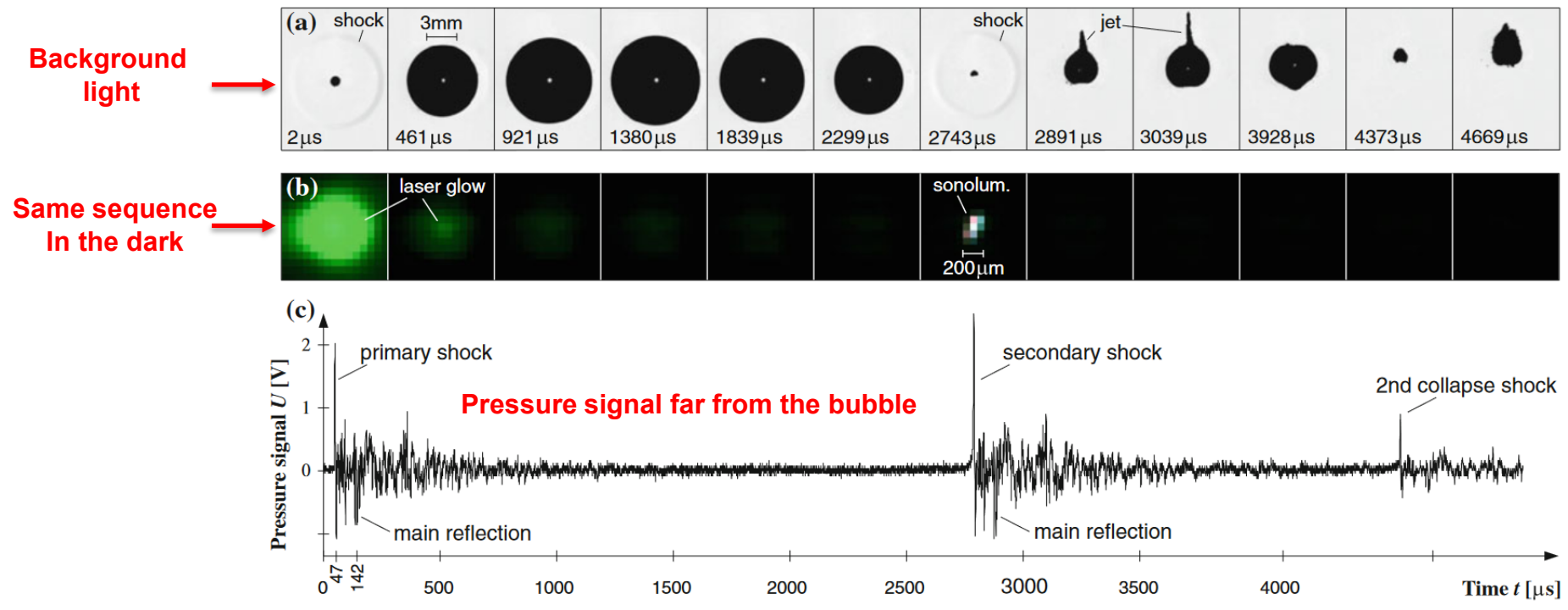
EPFL – Cavitation Research Group

Avenue de Cour 33 bis, 1007 Lausanne



Cavitation Bubble Dynamics

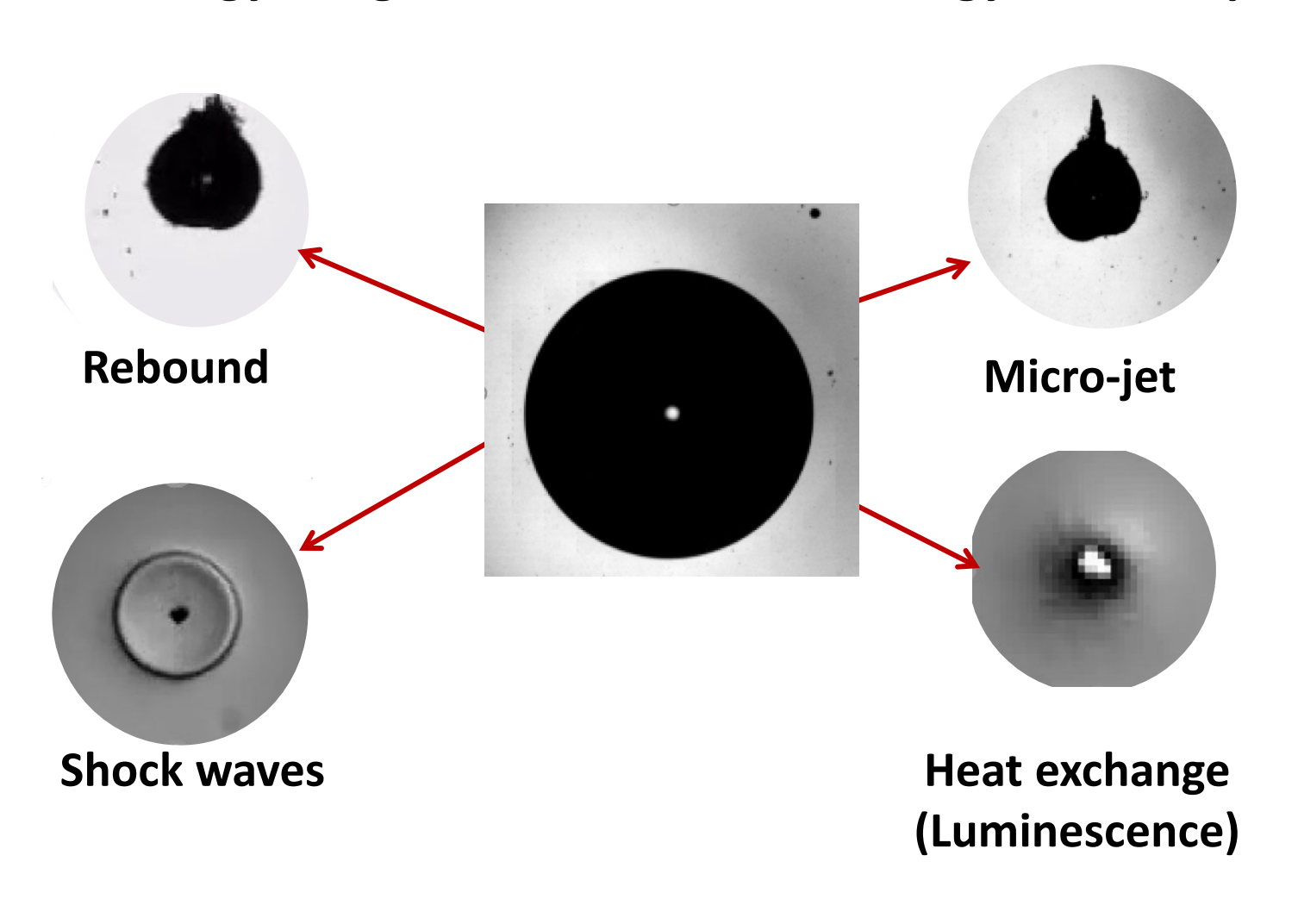
- Key phenomena associated with a laser-induced cavitation bubble:
 - Plasma → Explosive growth of the bubble with emission of a shockwave
 - ullet Deceleration of the expanding interface, up to $R=R_{max}\,\left(\dot{R}(R_{max})=0
 ight)$
 - Bubble collapses violently, leading to:
 - 1. Shockwave emission (compressibility effects)
 - 2. Micro-jetting, due to bubble deformation
 - 3. Bubble rebound (due to the non-condensable gas)
 - 4. Light (luminescence), due to extreme heating of the non-condensable gas





Cavitation Bubble Dynamics

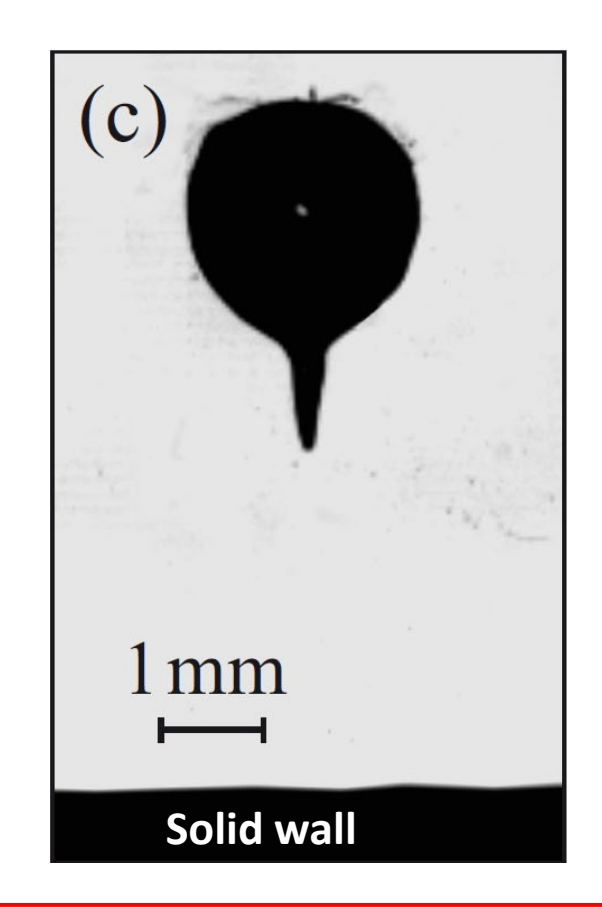
Energy budget: Where does the energy of a collapsing bubble go?

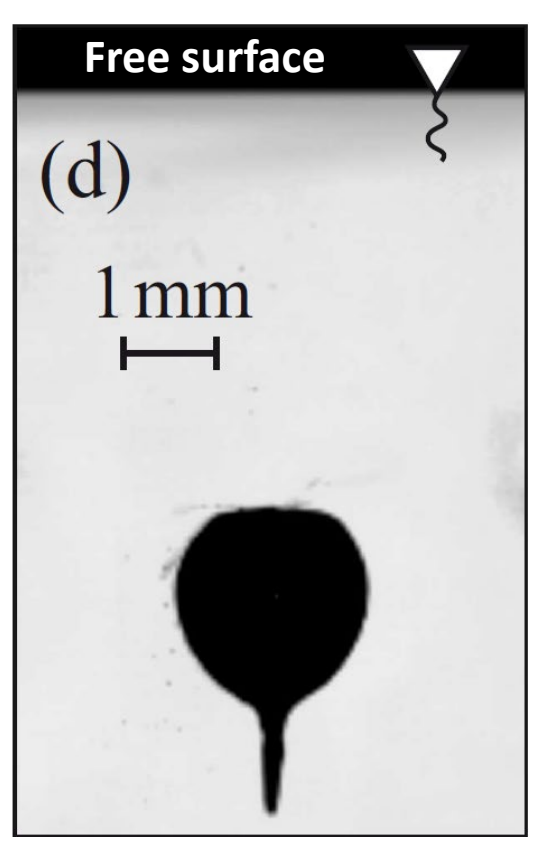


- Microjet
- Shock waves
- Luminescence
- Rebound

Cavitation Bubble Dynamics Microjets generated by collapsing bubbles

- Case of solid and free surfaces
 - Micro-jet due to pressure anisotropy
 - Well visible during the bubble rebound (conical shell of vapor)
 - Jet characteristics (size, speed, ...) \leftarrow pressure gradient?

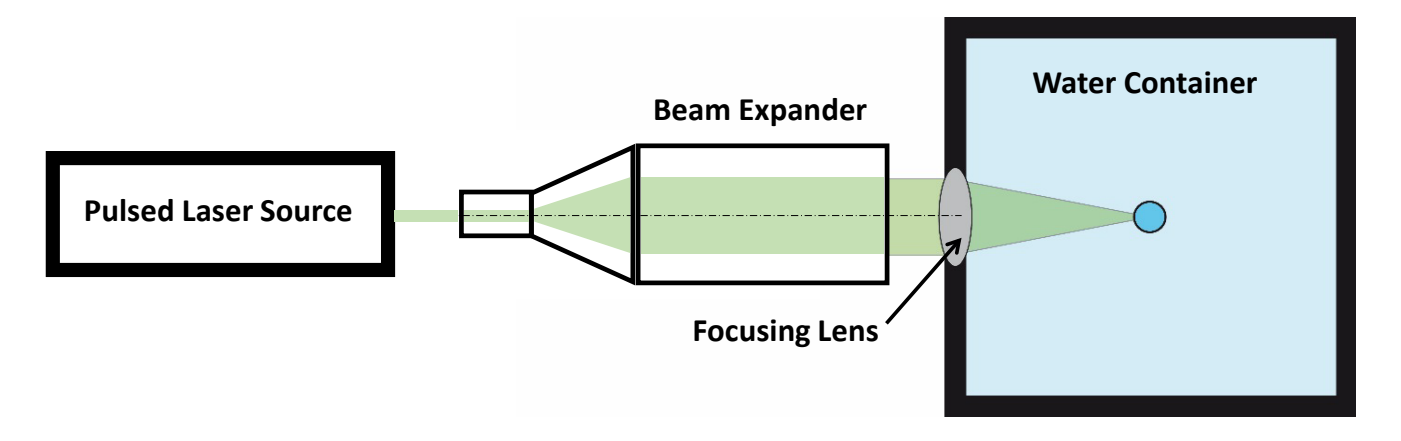




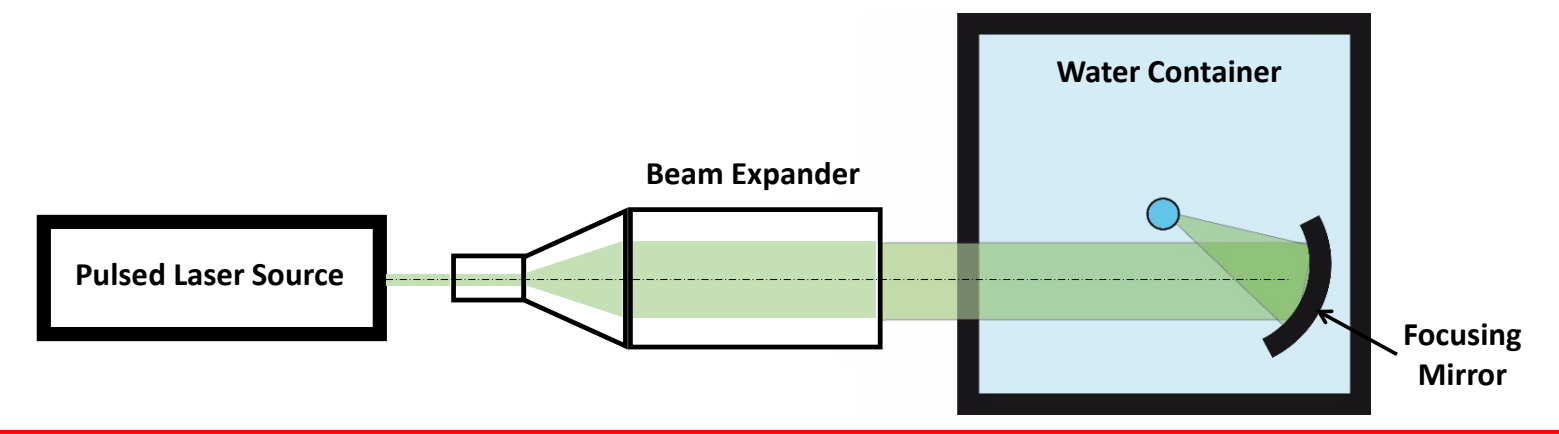


Chasing the most spherical bubble using Pulsed Focused Laser Technique

Classical Technique:



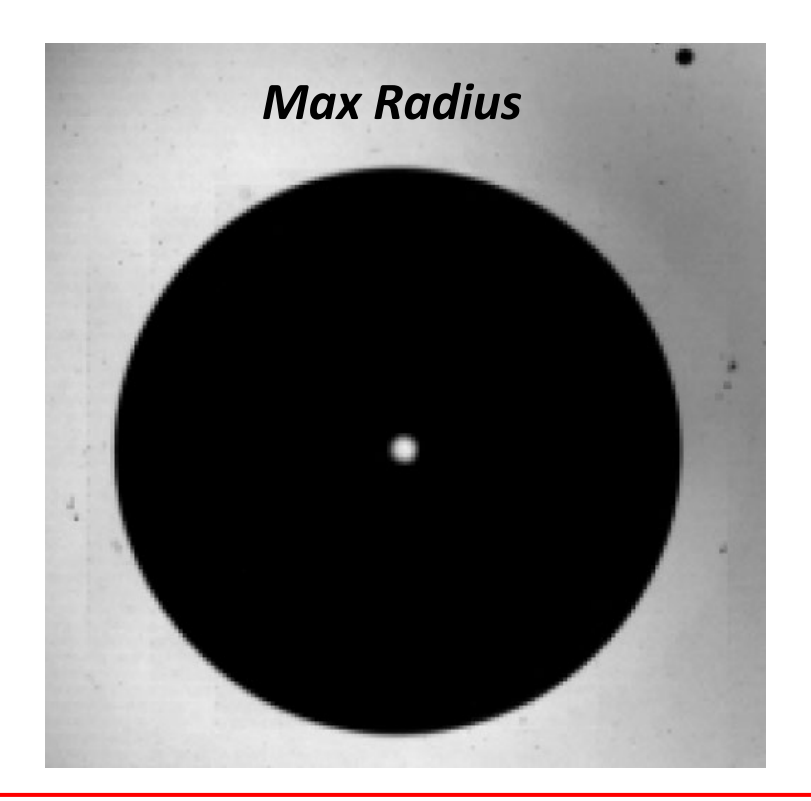
- Improved Technique: Immersed parabolic mirror
 - → less abberrations → better focusing → enhanced sphericity of the bubble

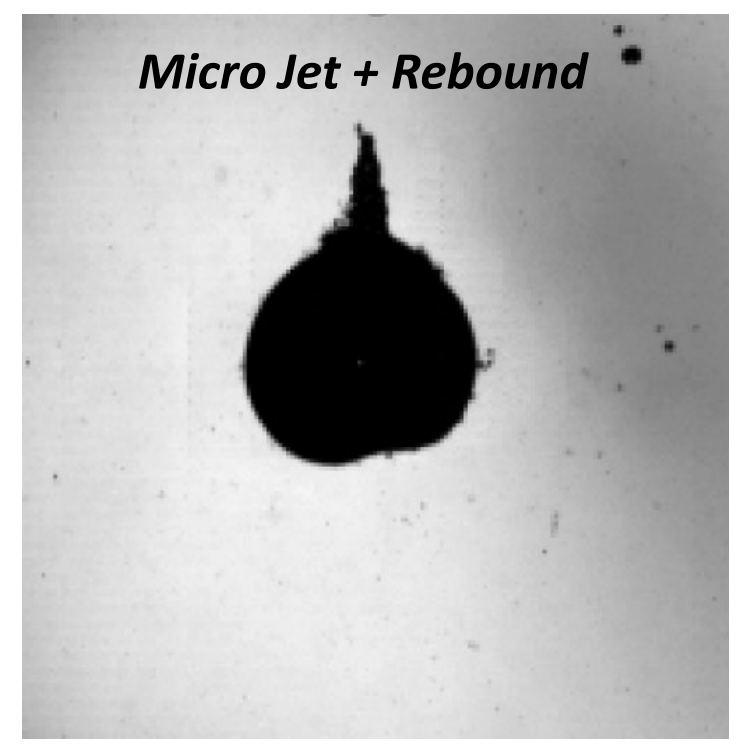




Chasing the most spherical bubble using Pulsed Focused Laser Technique

- Despite all the care given to the experimental setup, we always observe a deformation of the bubble when its maximum radius is in the millimeter range or above (under atmospheric pressure).
- This is due to the pressure anisotropy caused by the gravity field
 - The bottom of the bubble "feels" more pressure than its top

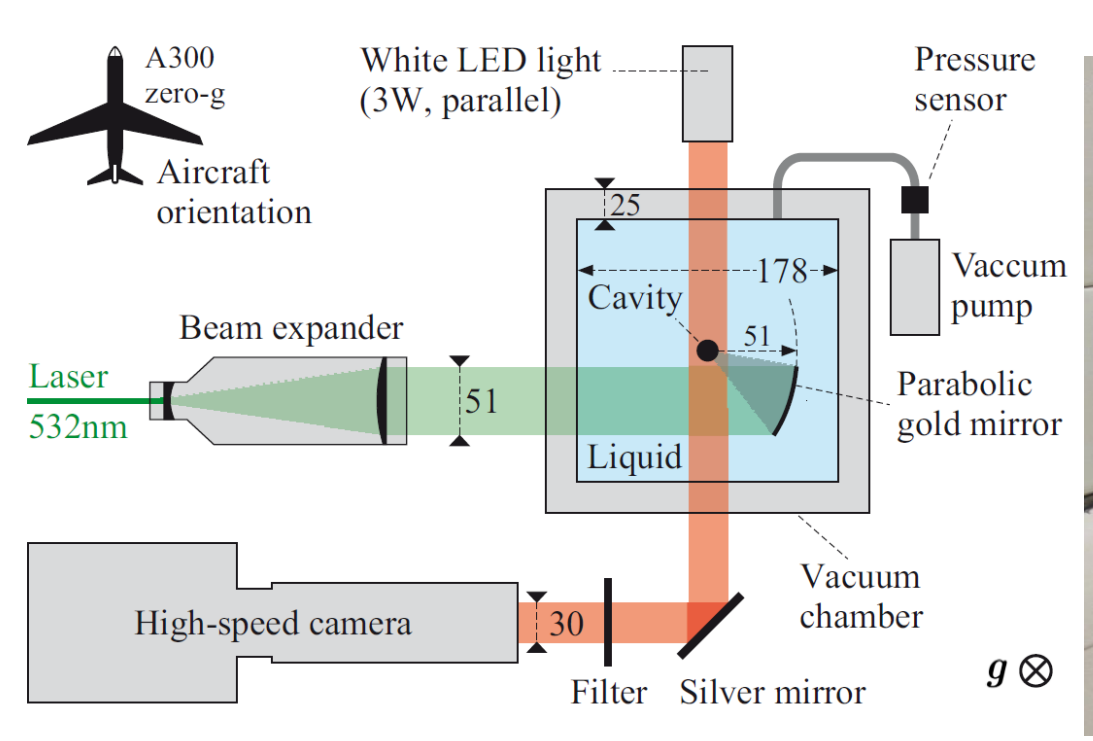






Effects of gravity induced pressure gradient

- Zero gravity tests: Experimental setup
 - Laser induced bubble in a closed water volume
 - Liquid pressure : varied from 8 to 80 Kpa
 - Point-like Plasma with a diameter < 0.1 mm
 - Pressure gradient: 0 to 18 KPa/m (gravity: 0, 1, 1.2, 1.4, 1.6, 1.8 g)



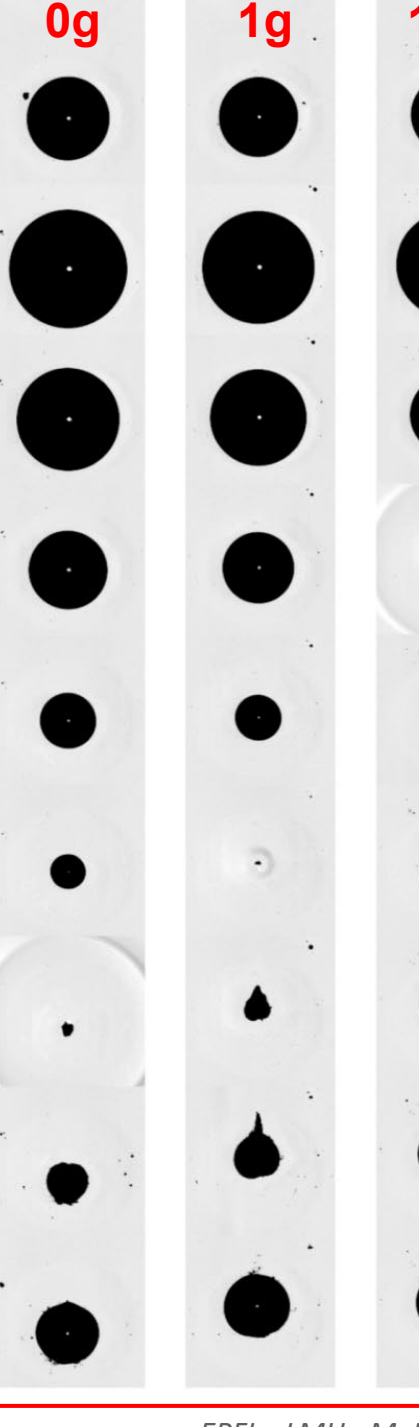




Effects of gravity induced pressure gradient

- Evidence of gravity induced jets (for the 1st time)
 - Upward jet due to gravity induced pressure gradient
 - More pronounced in hypergravity (1.8 g)
 - No jet is formed in microgravity

0g		1g		1.8g	
1748 μs	H 1 mm	3190 μs	H 1 mm	2956 μs	H 1 mm
Pressure = 28.50 kPa Max. radius = 4.519 mn	n	Pressure = 10.35 kPa Max. radius = 4.341 mm		Pressure = 11.58 kPa Max. radius = 4.490 mm	



Definition: Dimensionless pressure anisotropy parameter (vector):

$$\vec{\zeta} = -\frac{\vec{\nabla} p \ R_{max}}{\Delta p}$$

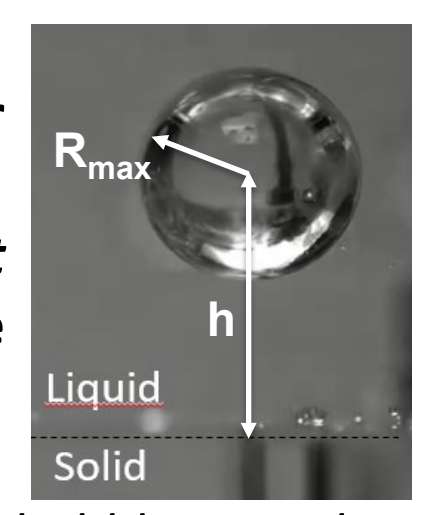
Where $\vec{\nabla} p$ is the pressure gradient "felt" by the bubble and Δp is the pressure difference between outside and inside the bubble $(p_{\infty}-p_{bubble})$

Pressure anisotropy induced by gravity:

$$|\zeta| = |\vec{\zeta}| = -\frac{|\vec{\nabla}p|R_{max}}{\Delta p} - \frac{\rho g R_{max}}{\Delta p}$$



- **Quantifying bubble asymmetry:**
 - How to characterize the pressure anisotropy in other configurations, such as neighboring rigid or free surfaces?
 - Kelvin Impulse theory (out of the scope of the present course¹), allows to relate the anisotropy parameter to the stand-off parameter $\gamma \left(= \frac{h}{R_{max}} \right)$



The Kelvin Impulse is the momentum gained by the liquid during bubble growth and collapse in a constant pressure gradient:

$$I = \nabla p \int_{-T_c}^{T_c} V dT$$

$$I = \frac{5\pi}{3\sqrt{6}} B\left(\frac{5}{6}, \frac{2}{2}\right) R_0^3 \sqrt{\Delta p \ \rho} \ \zeta \approx 4.789 R_0^3 \sqrt{\Delta p \ \rho} \ \zeta$$

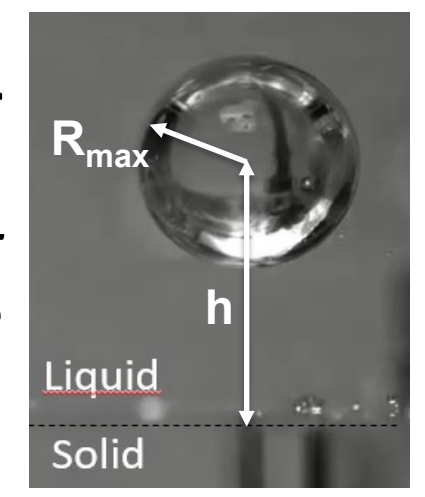
Where V is the volume of the bubble and B is the beta function, defined by:

$$B(x,y) = \int_0^1 t^{x-1} (1-t)t^{y-1} dt = \frac{\Gamma(x)\Gamma(y)}{\Gamma(x+y)}$$

¹ for more details, see Supponen et al. (2016) Journal of Fluid Mechanics



- Quantifying bubble asymmetry:
 - How to characterize the pressure anisotropy in other configurations, such as neighboring rigid or free surfaces?
 - Kelvin Impulse theory (out of the scope of the present course¹), allows to relate the anisotropy parameter to the stand-off parameter $\gamma\left(=\frac{h}{R_{max}}\right)$



The Kelvin Impulse is the momentum gained by the liquid during bubble growth and collapse in a constant pressure gradient:

driving pressure

$$\zeta = \begin{cases} -\rho \mathbf{g} R_0 \Delta p^{-1} \\ -0.195 \gamma^{-2} \mathbf{n} & \text{normal unit vector} \\ +0.195 \gamma^{-2} \mathbf{n} & \text{on surface} \\ -\rho (\mathbf{u} \cdot \nabla) \mathbf{u} R_0 \Delta p^{-1} \\ 0.195 \gamma^{-2} (\rho_1 - \rho_2) (\rho_1 + \rho_2)^{-1} \mathbf{n} \\ 0.195 \gamma^{-2} (4\alpha - 1 - 8\alpha^2 e^{2\alpha} E_1(2\alpha)) \mathbf{n} \end{cases}$$

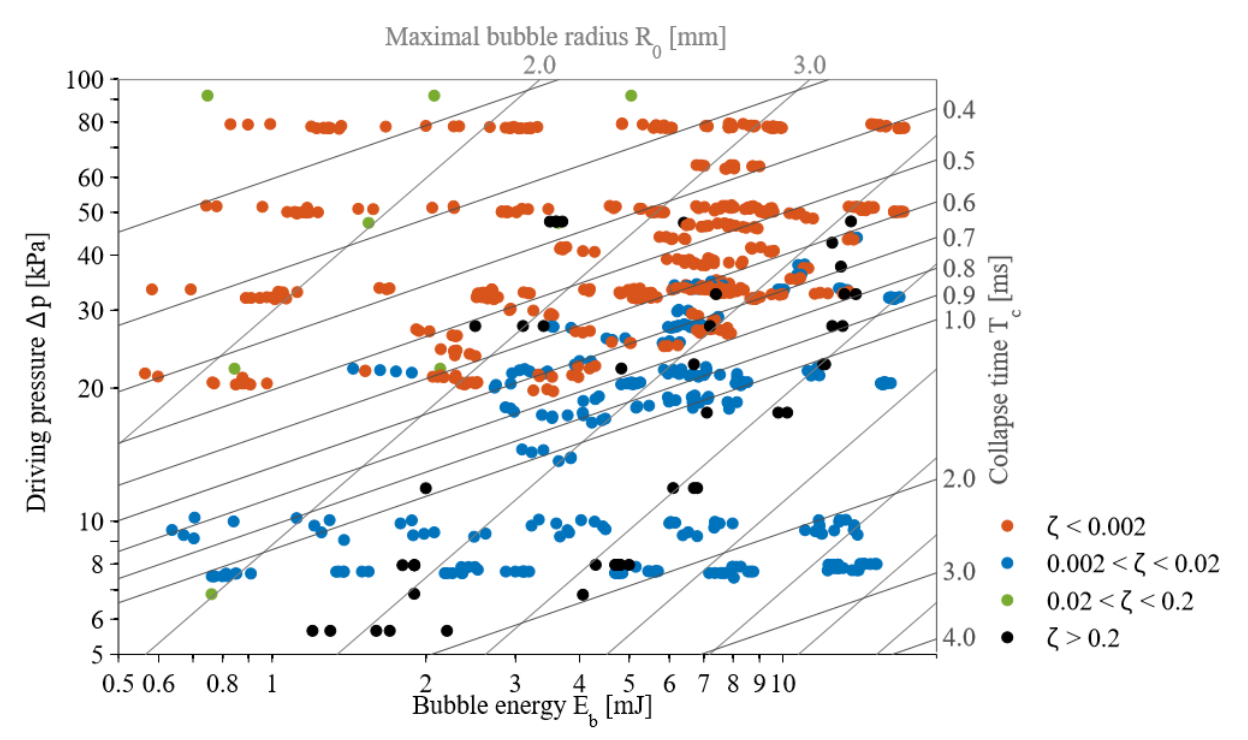
gravitational field
flat rigid surface
flat free surface
stationary potential flow
liquid interface
inertial boundary

 $\zeta = |\vec{\zeta}|$

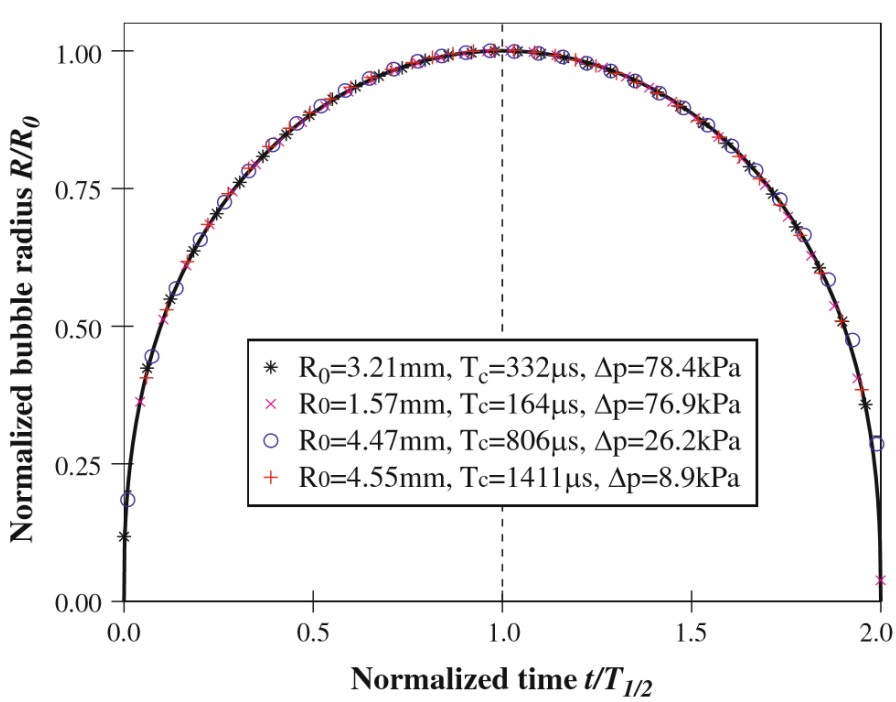
¹ for more details, see Supponen et al. (2016) Journal of Fluid Mechanics



- **Pressure anisotropy: Relevance?**
 - **Experimental validation:**
 - Overview of the parameter space covered by the experiment (gravity and a nearby rigid/free surface)



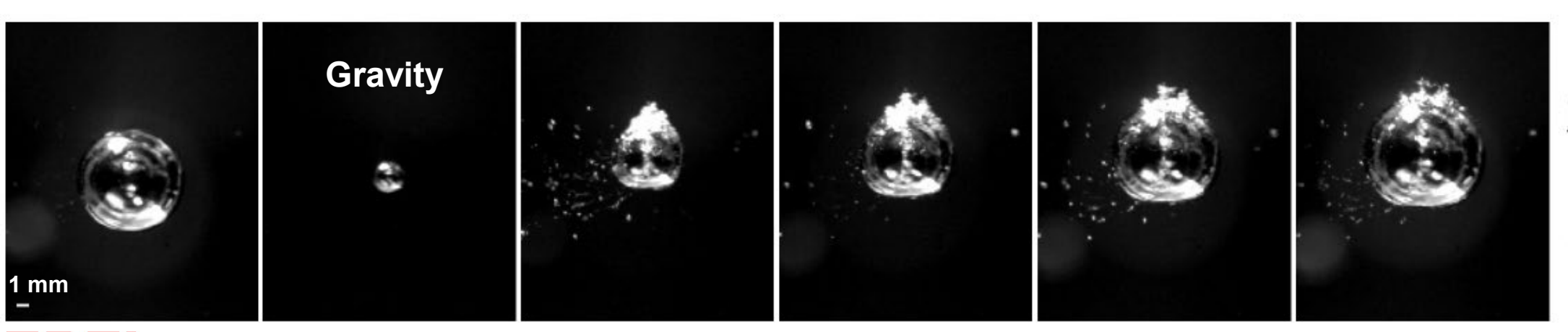
Rayleigh Model: A remarkable agreement



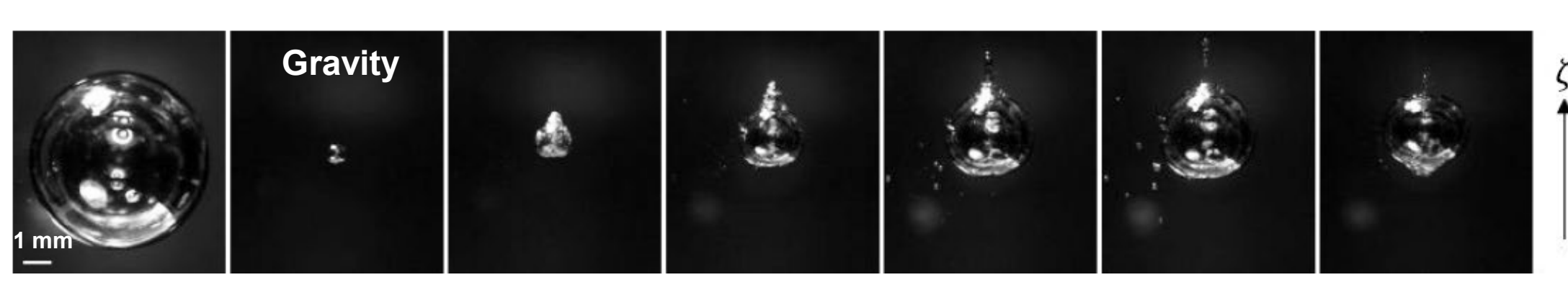
¹ for more details, see Supponen et al. (2016) Journal of Fluid Mechanics



- Jet types:
 - 1st type: Weak Jets $(\zeta < 10^{-3})$:
 - Slight deformation of the bubble
 - The jet hardly pierces the intefrace and remains within the bubble throughout the collapse and rebound phases.



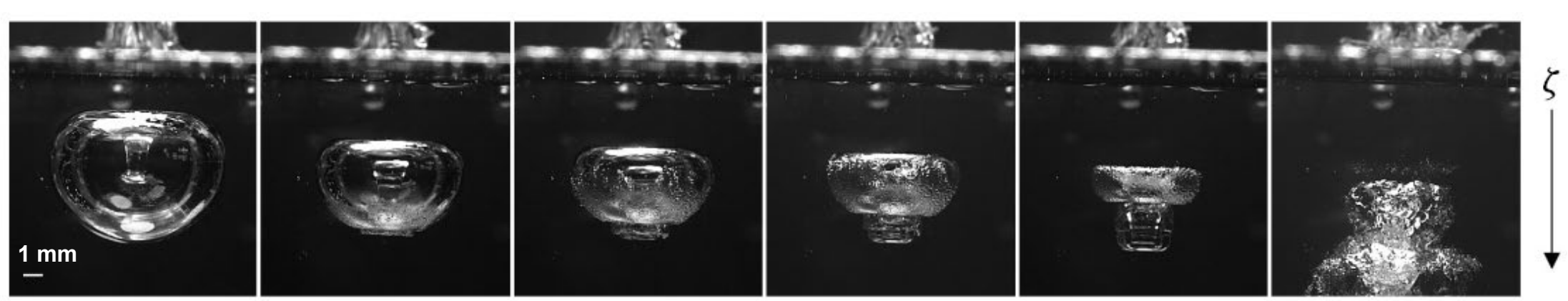
- Jet types:
 - 2^{nd} type: Intermediate jets $(10^{-3} < \zeta < 0.1)$:
 - The bubble deforms significantly at the end of the collapse phase
 - The jet pierces the bubble and clearly emerges during the rebound phase



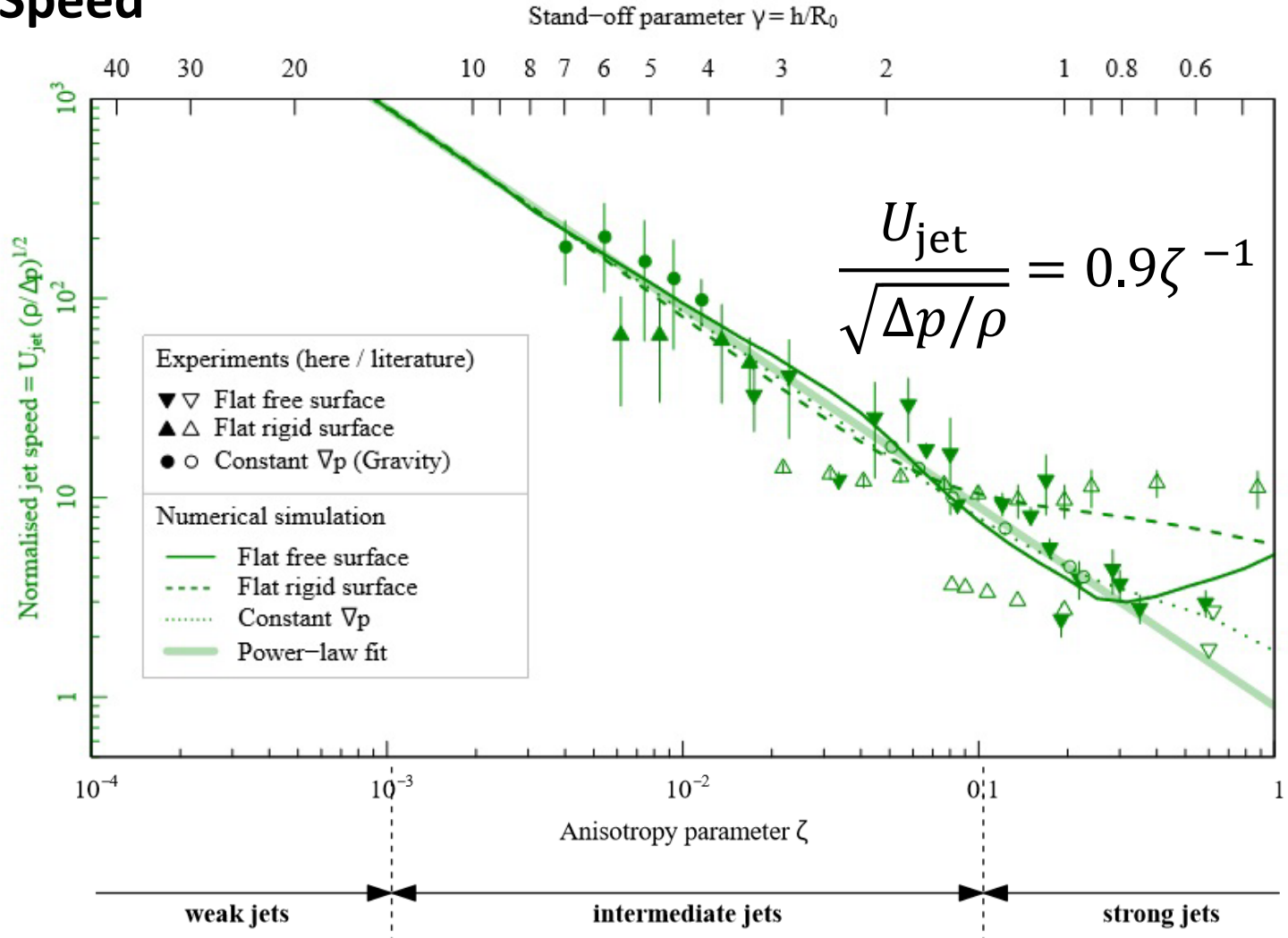
¹ for more details, see Supponen et al. (2016) Journal of Fluid Mechanics

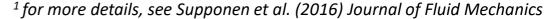


- Jet types:
 - 3rd type: <u>Strong jets</u> (ζ > 0.1) :
 - The bubble deforms signficantly early in the collapse phase
 - The jet pierces the bubble "long time" before the collapse

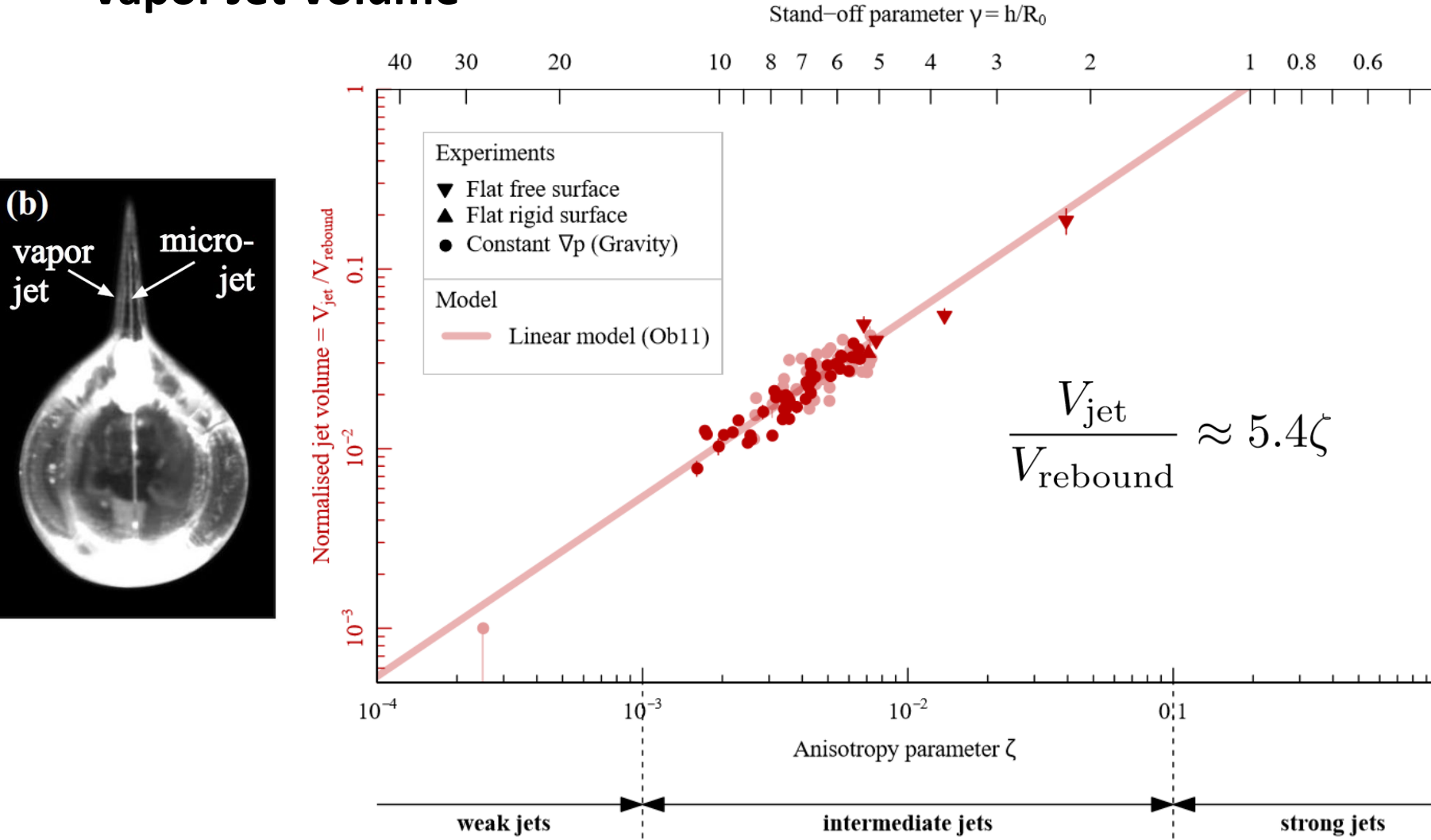


Jet Speed





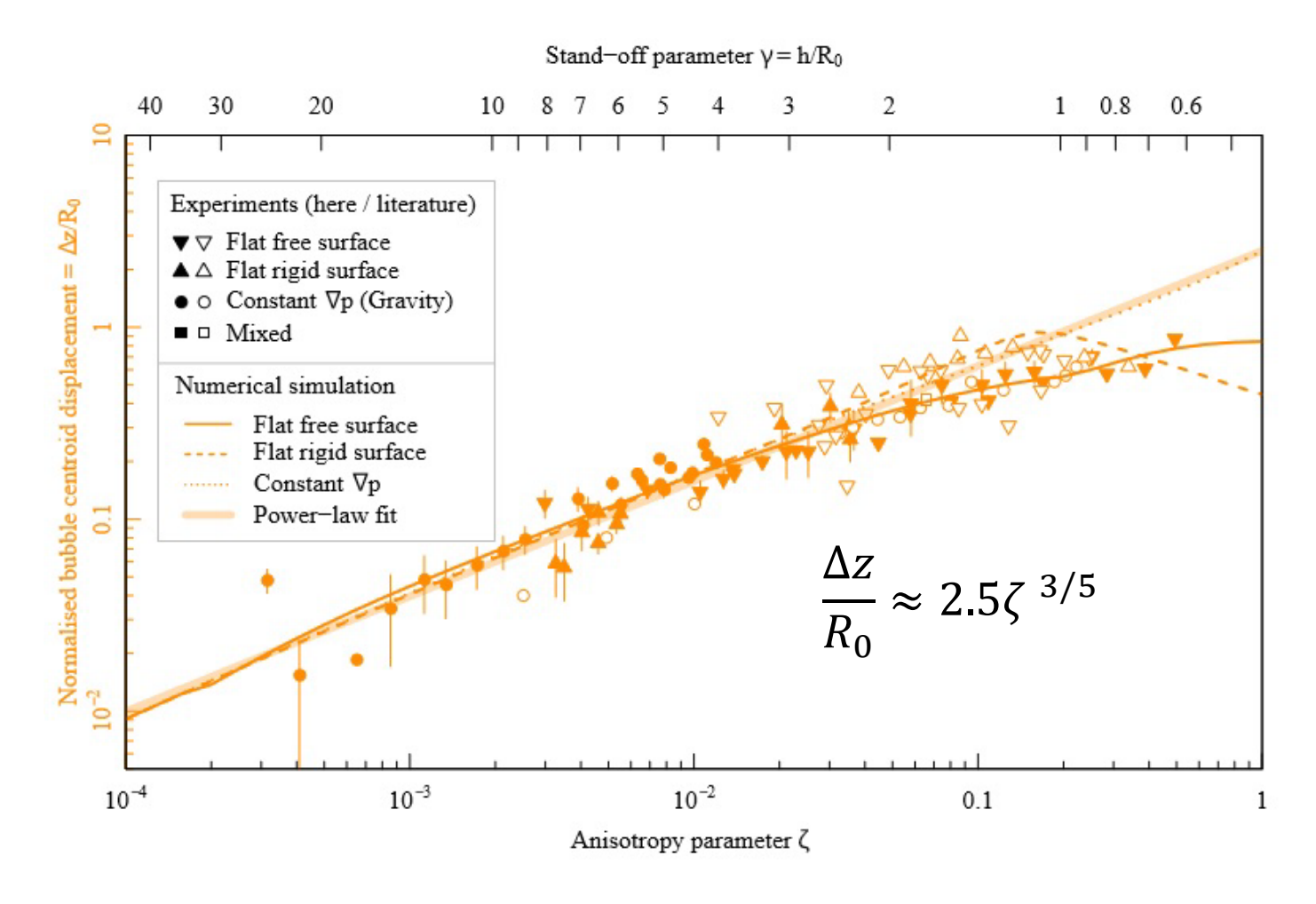
Vapor Jet Volume

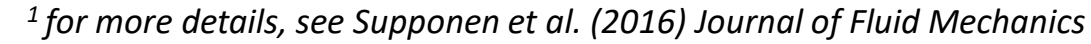


¹ for more details, see Supponen et al. (2016) Journal of Fluid Mechanics



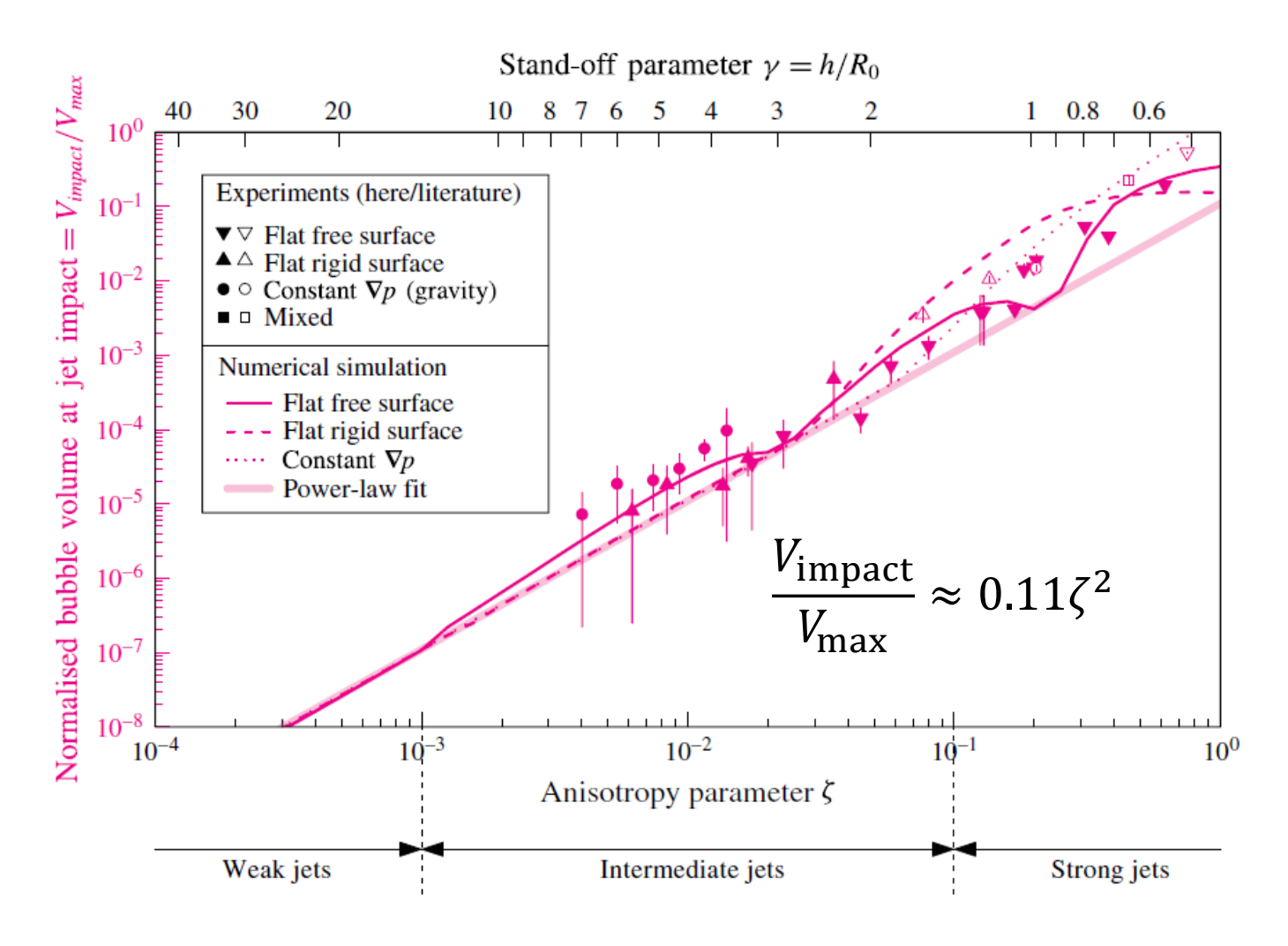
• Bubble centroid displacement

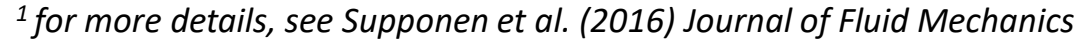


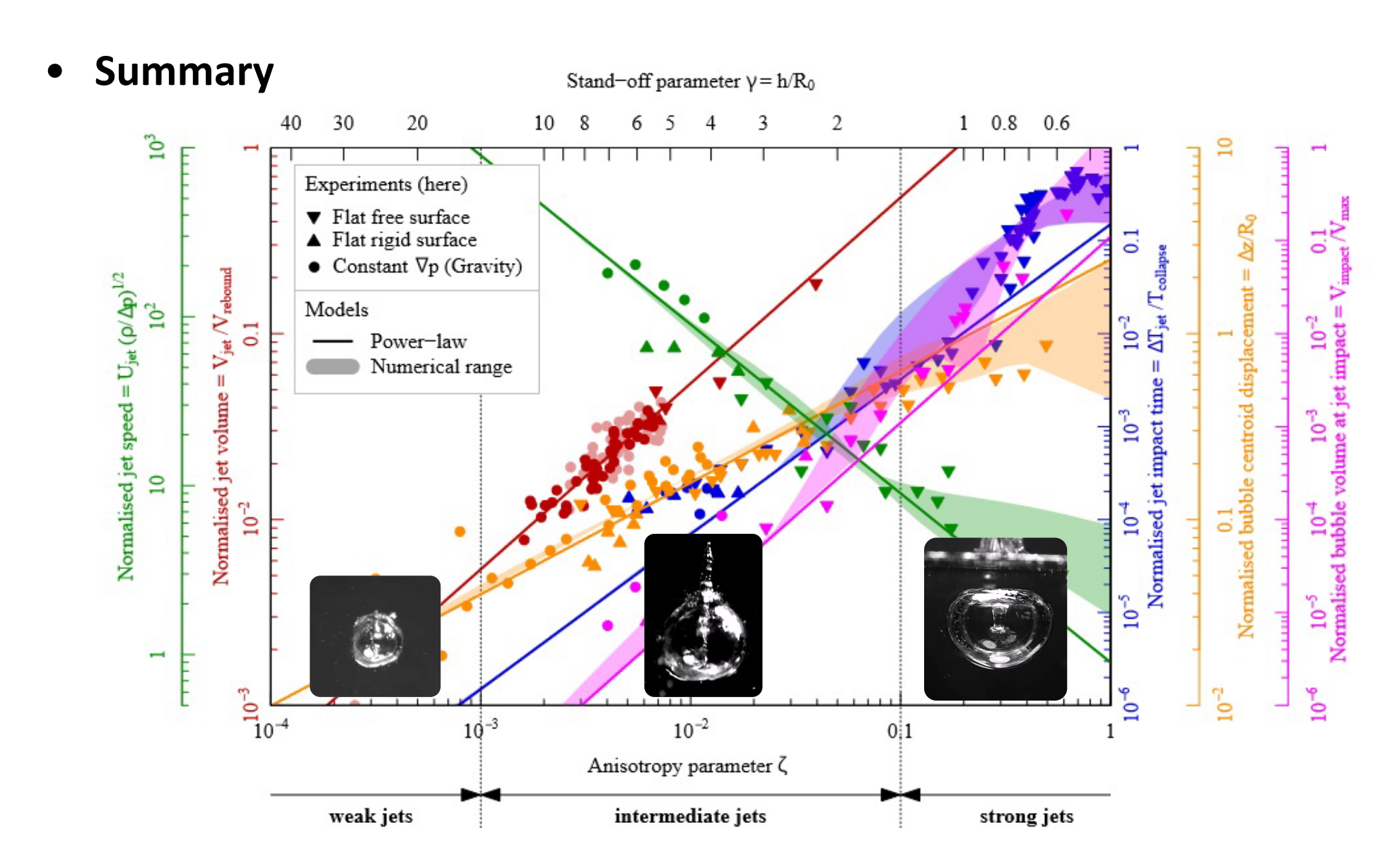


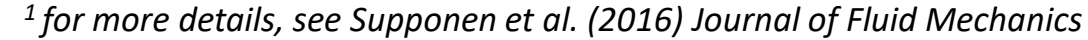
Bubble volume at jet impact

Bubble volume at jet impact









Bubble Dynamics: Jet shapes by potential flow computation

- Flow simulation of a collapsing bubble near boundaries :
 - Boundary integral method
 - Experimental validation

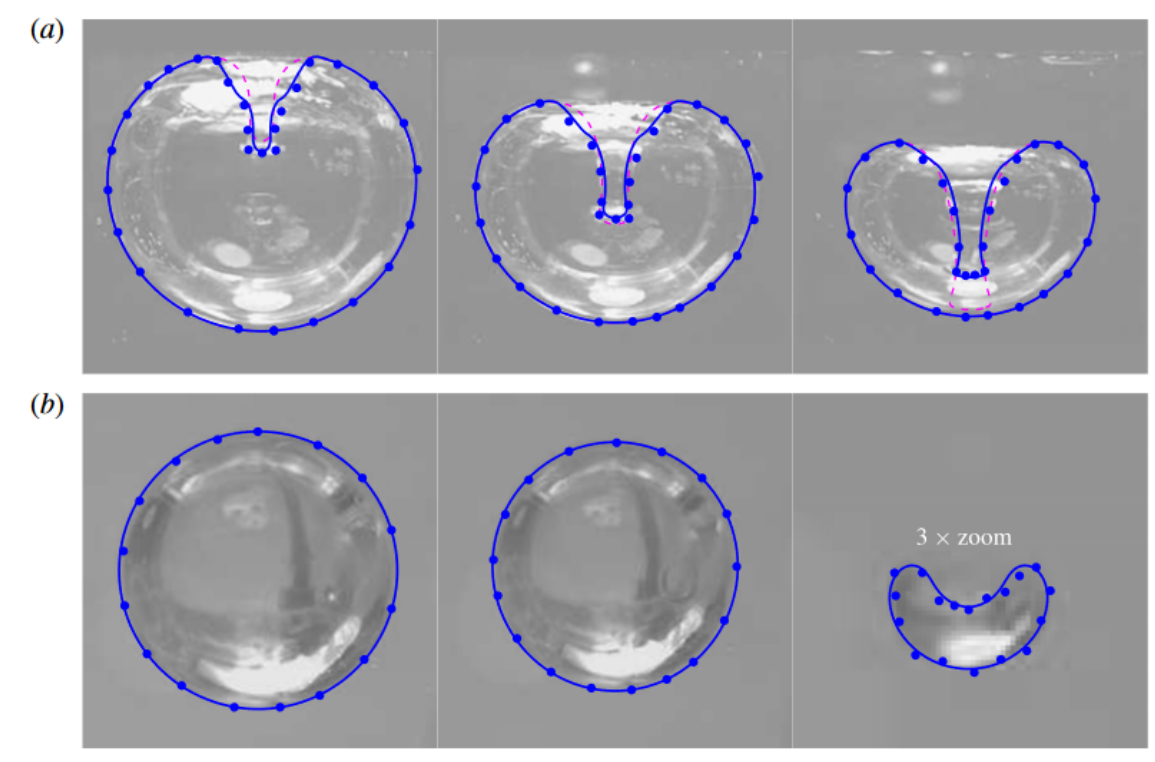


FIGURE 11. (Colour online) The numerical simulations superimposed on the experimental visualisations for a bubble collapsing near a free surface $\gamma = 0.56$ (a) and near a rigid surface $\gamma = 2.32$ (b). The blue points are extracted from the observed bubble shapes and the lines represent simulated data. In (a), the simulated bubble shape (dashed purple line) was corrected for optical refraction (solid blue line) by the outer bubble boundary, assuming a refraction by a sphere with equations analogous to those in Kobel et al. (2009) (with water and vacuum inverted).

¹ for more details, see Supponen et al. (2016) Journal of Fluid Mechanics



Bubble Dynamics: Jet shapes by potential flow computation

 Role of the jet driver (rigid boundary, free surface, gravity) on the shape of the jet induced by a collapsing bubble:

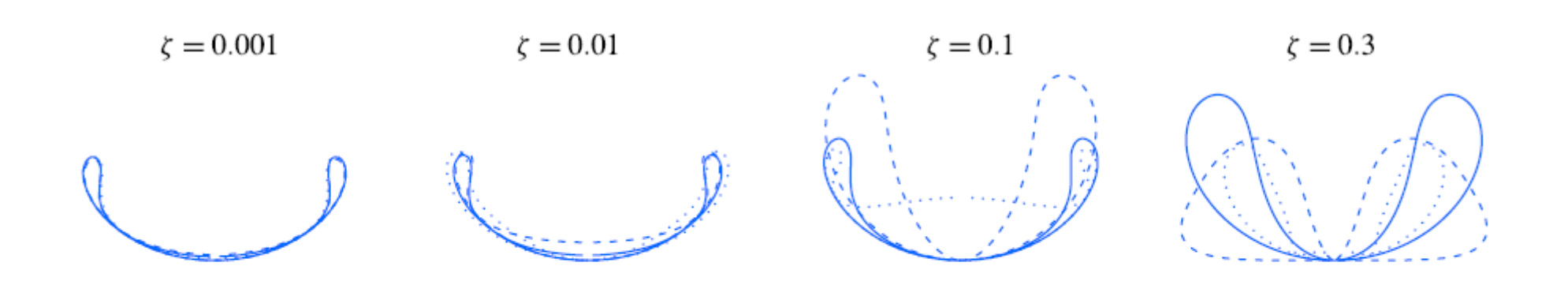


FIGURE 13. (Colour online) Zoomed bubble shapes at the jet impact from figure 12. The different jet drivers are indicated by solid (constant ∇p), dashed (rigid surface) and dotted (free surface) lines.

$$\begin{split} \Delta T_{jet}/T_{collapse} &= 0.15 \, \zeta^{5/3} & \text{(normalised jet impact time),} \\ U_{jet}/(\Delta p/\rho)^{1/2} &= 0.9 \, \zeta^{-1} & \text{(normalised jet speed),} \\ \Delta z/R_0 &= 2.5 \, \zeta^{3/5} & \text{(normalised bubble displacement),} \\ V_{impact}/V_{max} &= 0.11 \, \zeta^2 & \text{(normalised bubble volume at jet impact),} \\ V_{jet}/V_{rebound} &= 5.4 \, \zeta & \text{(normalised volume of vapour-jet).} \end{split}$$

Power laws

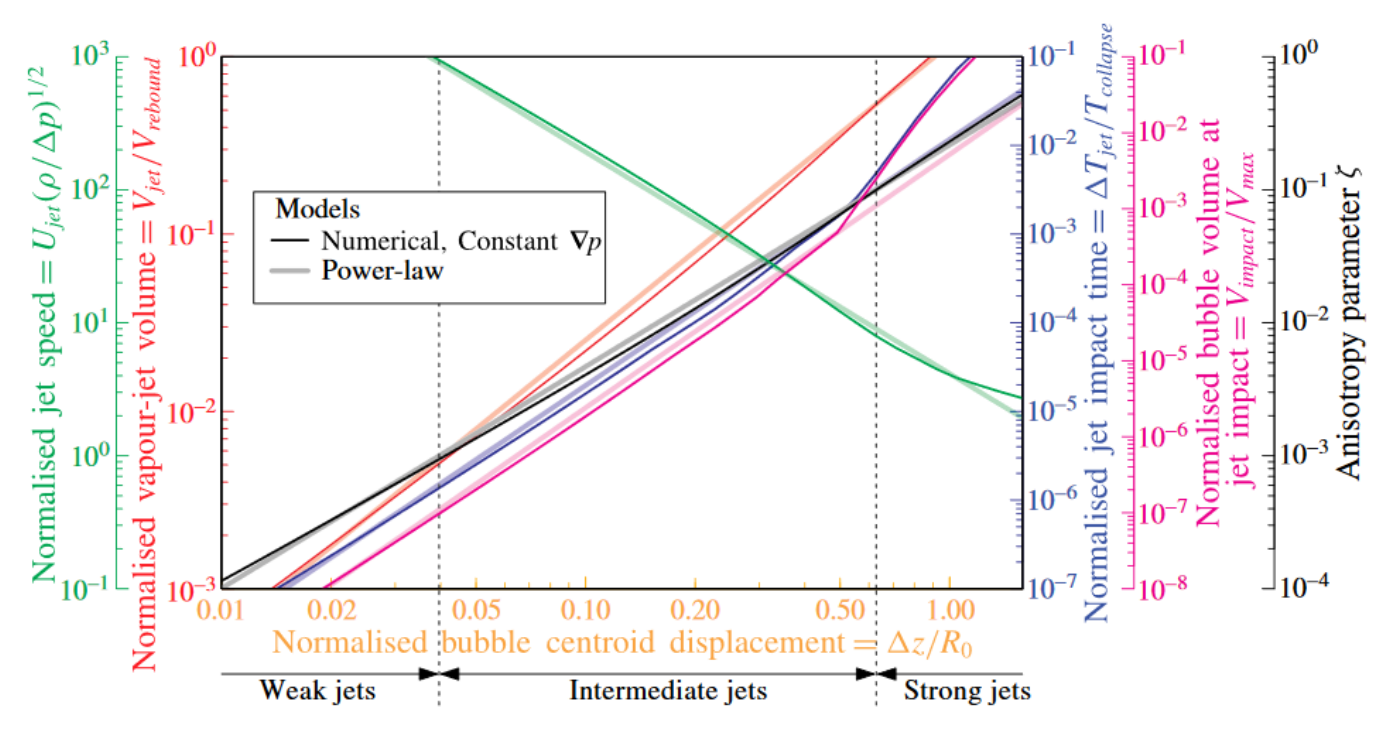


FIGURE 20. The pressure anisotropy parameter ζ and the normalised jet impact time, the normalised jet speed, the normalised bubble volume at jet impact and the normalised jet volume (Obreschkow *et al.* 2011) are plotted as functions of the normalised bubble centroid displacement for jets driven by a constant pressure gradient. The simulated models and the power-law fits are plotted with dark and light lines, respectively.

PhD Thesis, Armand Sieber, 2023

Motivations:

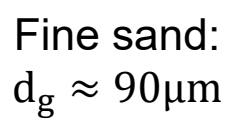
- Cavitation bubble dynamics $\leftarrow \rightarrow$ granular media dynamics.
 - Compelling scientific interest with rich physics.
- Applications in the field of underwater explosions, when the charges are detonated near the seafloor.
 - o Information about the bubble acoustic signature (Krieger et al, 2005).

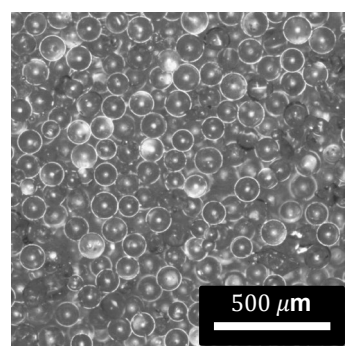
Method:

 Experimental investigation laser-induced cavitation bubbles near beds of sand with different grain sizes.

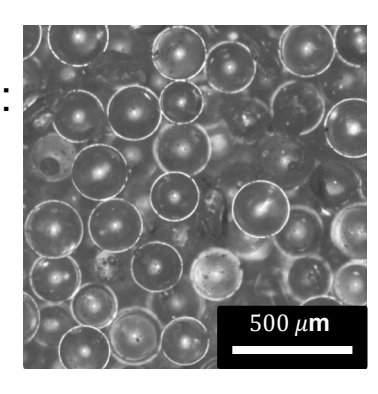
Granular boundaries → experiment:

■ Beds of sand made out of soda lime glass beads \rightarrow 3 granularities investigated:

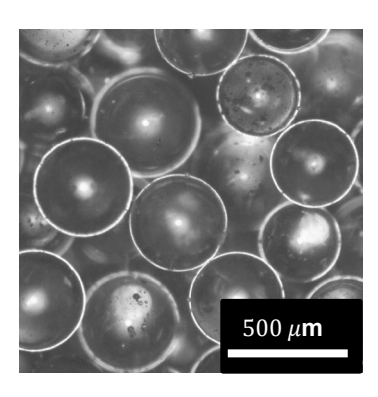




Medium sand: $d_{\mathbf{g}}\approx 200\mu m$

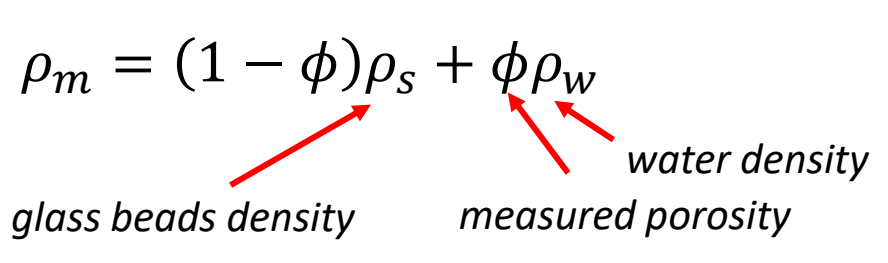


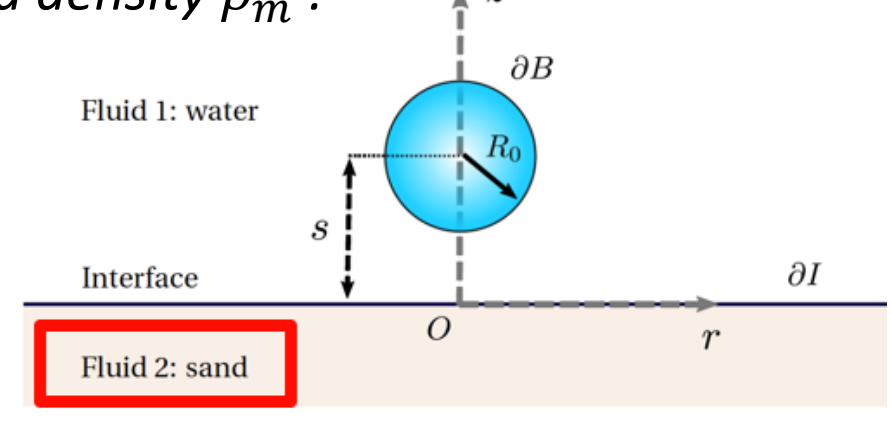
Coarse sand: $d_g \approx 350 \mu m$



Granular boundaries → simulation (BIM):

lacktriangle Water-saturated sand treated as a fluid with a density ho_m :







Impact of the standoff distance \rightarrow 3 regimes depending on γ

 $\gamma pprox 5.3$ $\gamma pprox 1.3$ $\gamma pprox 0.6$ Decreasing γ

First regime:

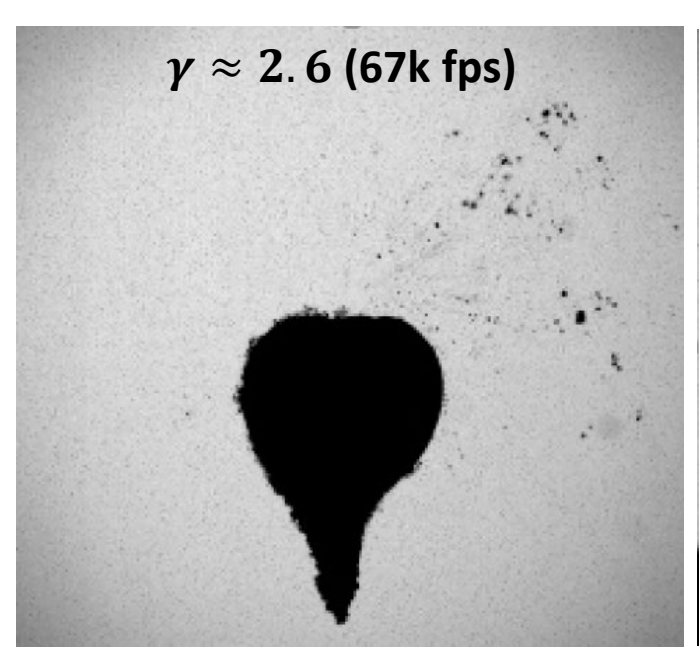
- No influence of grain size.
- Simualtions fairly reproduce bubble dynamics.

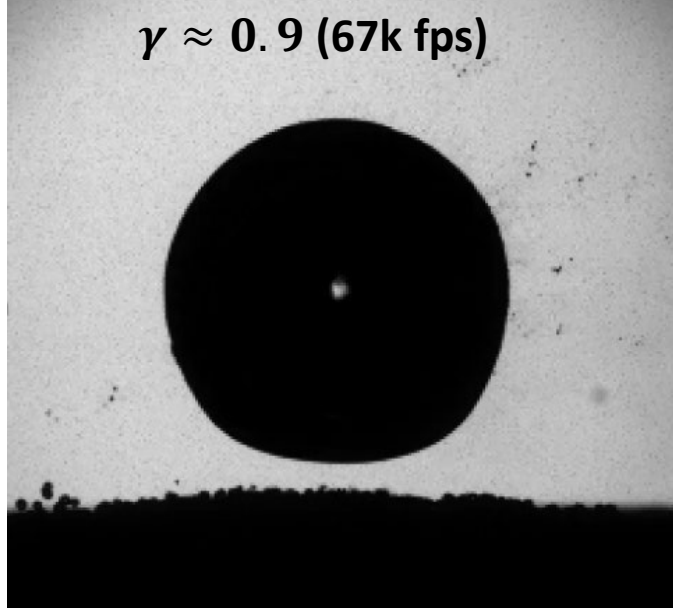
Second regime:

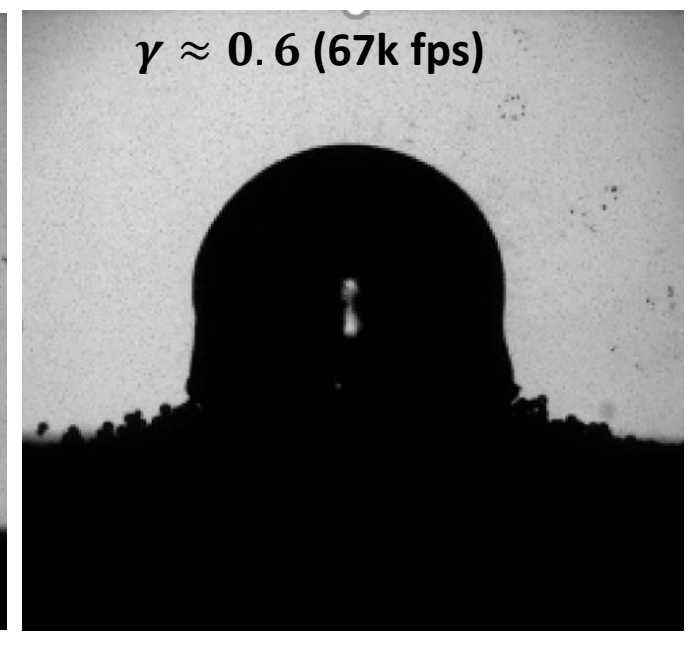
- Bubble's rebound 'swallowed' by sand.
- Sand grain size matters.

Third regime:

- Bubble 'swallowed' by sand.
- Sand grain size matters.

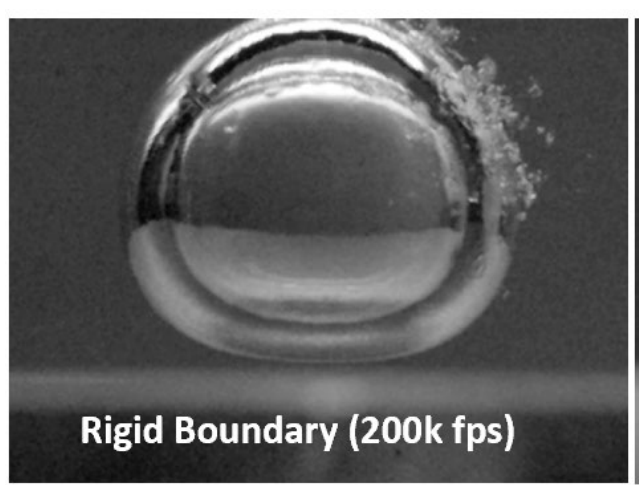


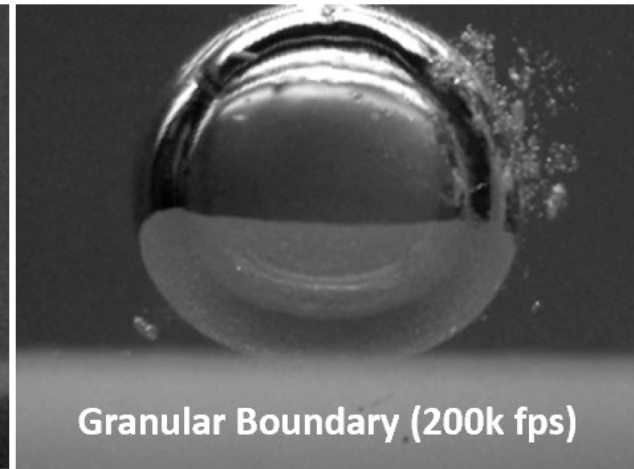




Results: second regime 1. $3 > \gamma > 0$. 6

Bubbles dynamics at $\gamma \approx 0.8$ ($R_{max} = 4.4$ mm)



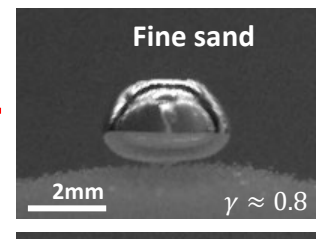


- Formation of a granular mound upon bubble collapse.
- Bubble takes on a conical shape.
- Bubble rebound 'swallowed' by sand.

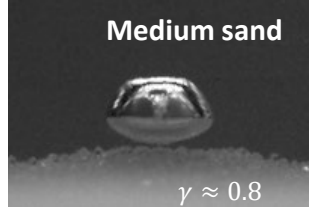
• Effect of the sand grain size on the bubble shape and microjet speed:

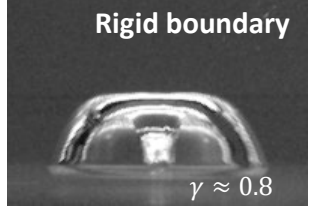
$$v_{jet} = 328 \, m/s$$
 \leftarrow

$$v_{jet} = 218 \, m/s$$
 \leftarrow







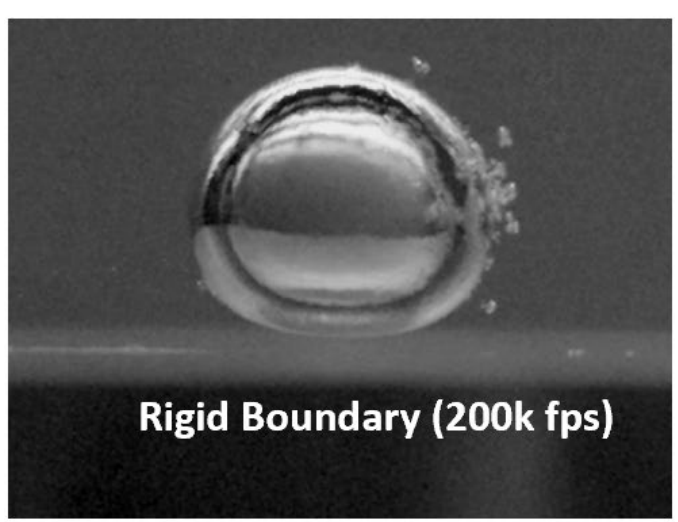


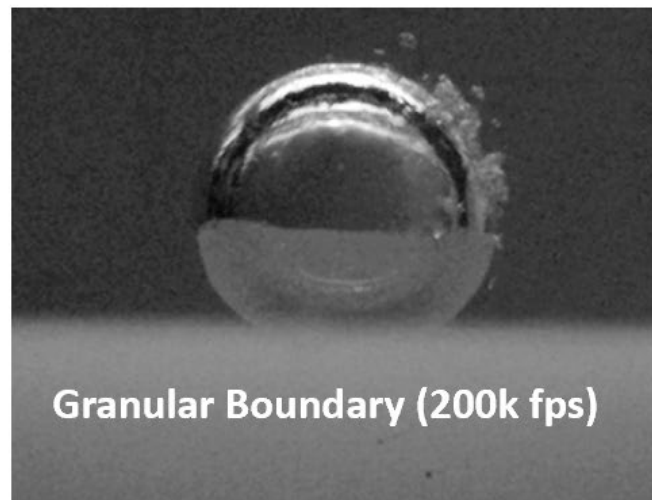
$$\rightarrow v_{jet} = 289 \, m/s$$

- $\rightarrow v_{jet} = 87 \, m/s$
- Finer sand → larger bubble volume at microjet impact.
- Finer sand → faster and thiner microjets.

Results: third regime $0.6 > \gamma > 0.3$

Bubbles dynamics at $\gamma \approx 0.5$ ($R_{max} = 4.4$ mm)

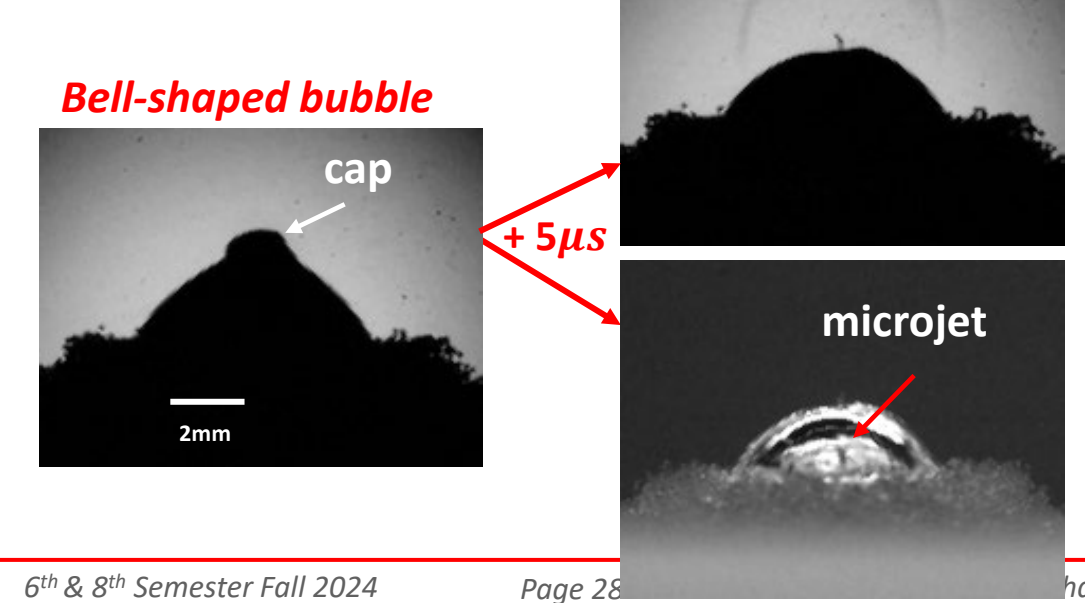




- Bubble takes a bell-shape.
- Bubble 'swallowed' by sand
- Bubble rebounds within the sand
- Formation of a post-collapse crater

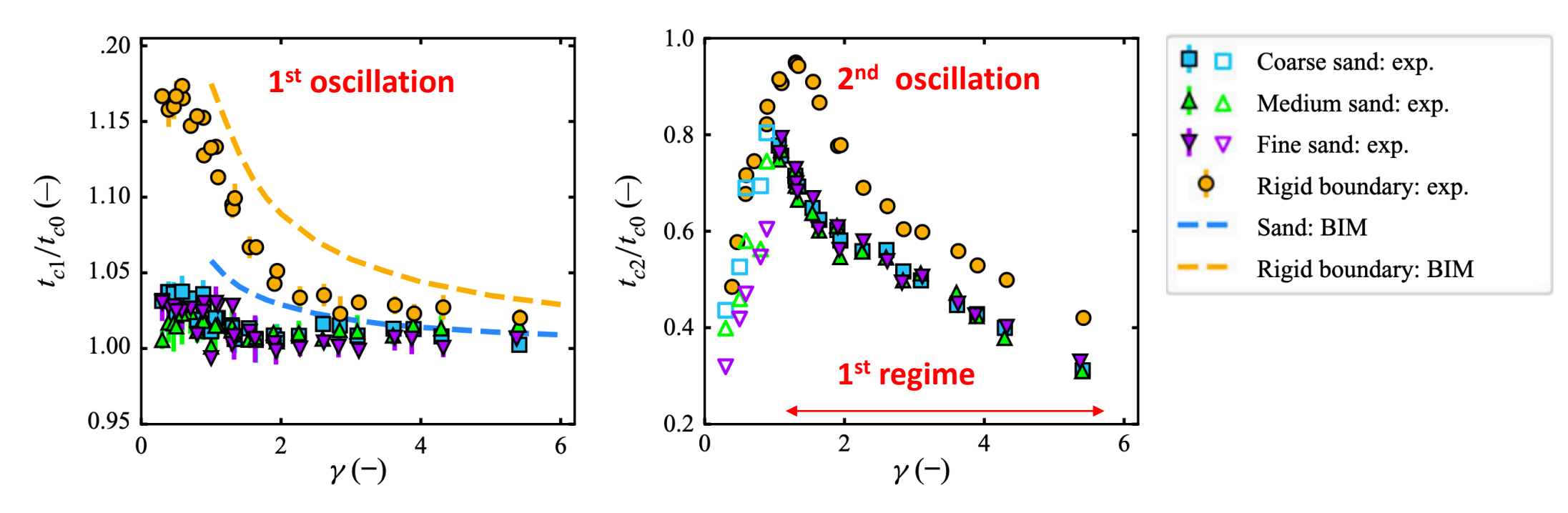
- Final instants of the bubble collapse:
 - The bell-shaped bubble cap collapses faster than the rest of the bubble
 - → Emission of a shockwave
 - \rightarrow Very fast microjet : ~1000 m/s !

Cavitation & Interface Phenomena: Chap 3.2





Results: bubble 1st and 2nd oscillation periods (t_{c1} and t_{c2})



Weak influence of the sand grain size.

Cavitation & Interface Phenomena: Chap 3.2

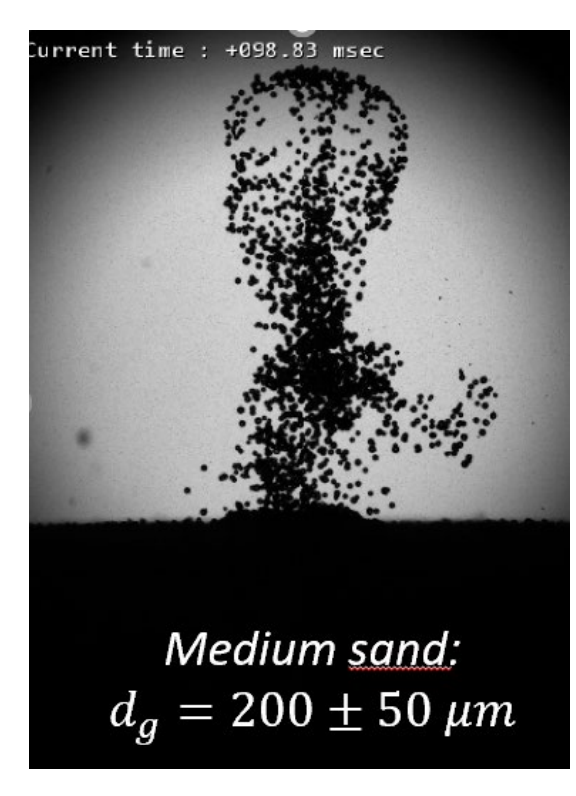
Bubble oscillations are longer near a rigid boundary.

$$t_{c0} = 1.83 R_{max} \sqrt{\rho/\Delta p}$$
 (2x Rayleigh collapse time)



Granular boundaries: jets of sand







Two possible mechanisms may explain the sand jetting:

- 1. Rebound of the bubble below the sand surface creates a cavity in the granular medium → collapse of the cavity → formation of a jet of sand that shoots upwards
- 2. Flow field induced by the collapsing bubble \rightarrow ascending vortex ring observed after the toroidal 2nd collapse of bubbles near rigid boundaries (Reuter et al., 2017).

Ref.: Sieber et al. Dynamics of cavitation bubbles near granular boundaries. J. of Fluid Mech., 2022.



PhD Thesis, Armand Sieber, 2023

Motivations:

- Various applications in biomedicine where bubbles may interact with human tissues:
 - Targeted drug delivery (Stride et Coussios, 2019).
 - Ultrasound-based tissue ablation (Bader et al., 2019).
 - Laser-based medical procedures, e.g. laser lithotripsy (Ho et al., 2021) or laser atherectomy (Golino et. al, 2019).

Method:

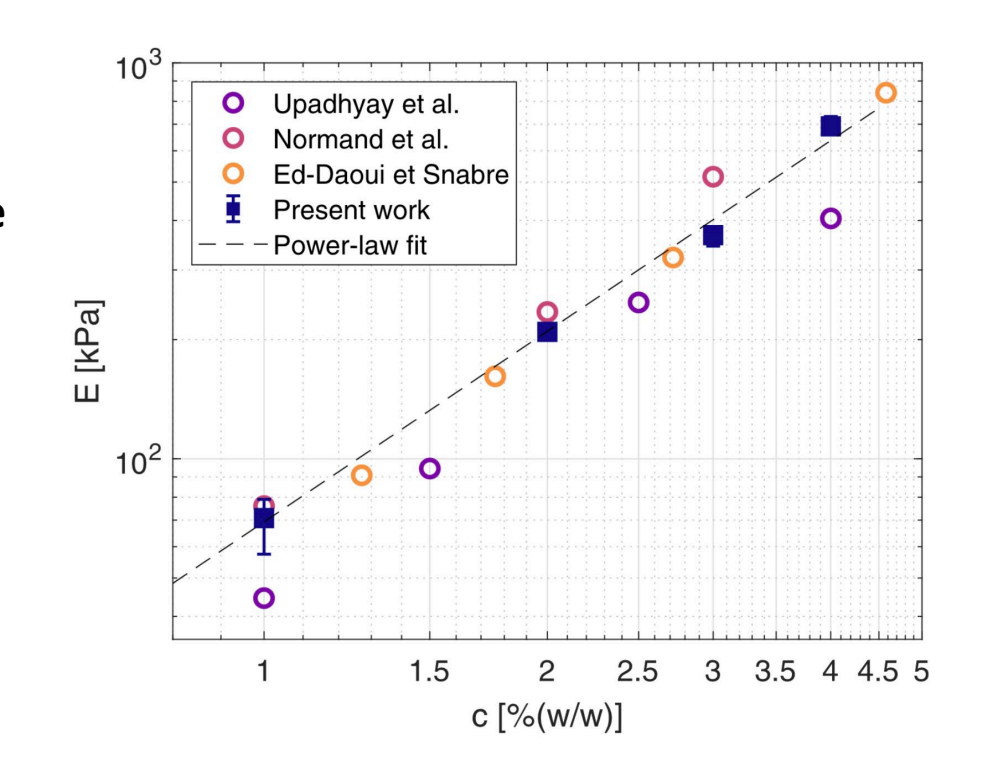
 Simplified test case: study of millimetric cavitation bubbles near initially flat, tissue-mimicking boundaries with different levels of elasticity.



Interactions of cavitation bubbles with tissue-mimicking materials

→ We used agarose hydrogels

- Agarose hydrogels with different agarose concentration c: 1%, 2%, 3% and 4% w/w.
- Uniaxial compression tests \rightarrow as c is increased the Young's modulus E increases.
- Power-law scaling: $E = 69.9c^{1.6}$ kPa
- Hydrogels mimic different human tissues, e.g. :
 - Cardiac muscle cells $\rightarrow E \sim 100 \text{ kPa}$
 - Cornea \rightarrow $E \sim 290 \text{ kPa}$
 - Gastrointestinal tissues \rightarrow $E \sim 320 790 \text{ kPa}$



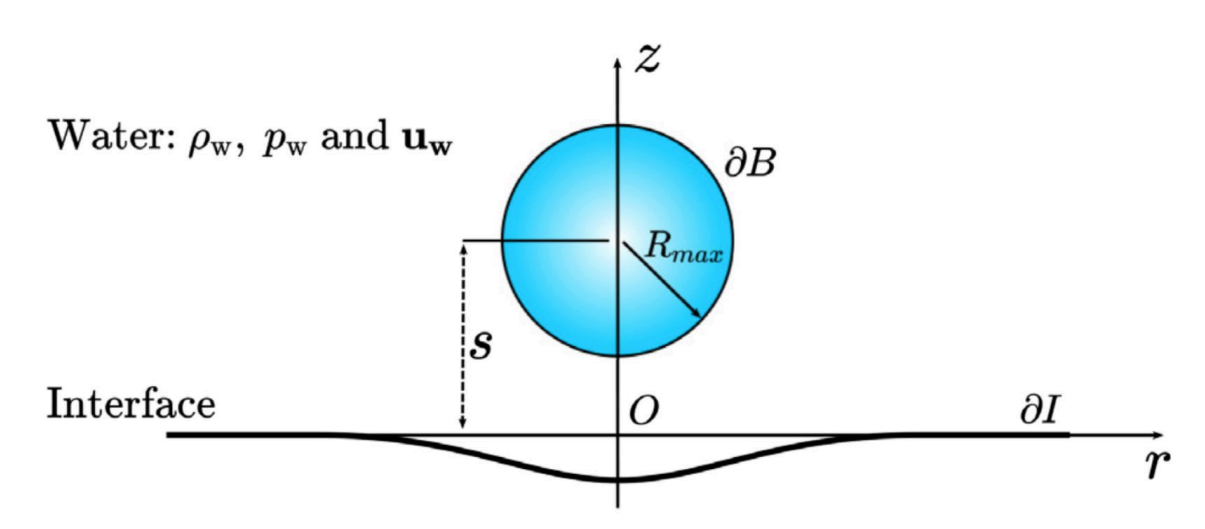
- Numerical method: Boundary Integral Method (BIM)
 - Agarose hydrogel modelled as a liquid with density ho_a ,

$$\rho_a = \frac{c\rho_s + (100 - c)\rho_w}{100}$$

Elasticity of the hydrogel modelled as an interfacial surface tension,

Derived from an energy balance reasoning

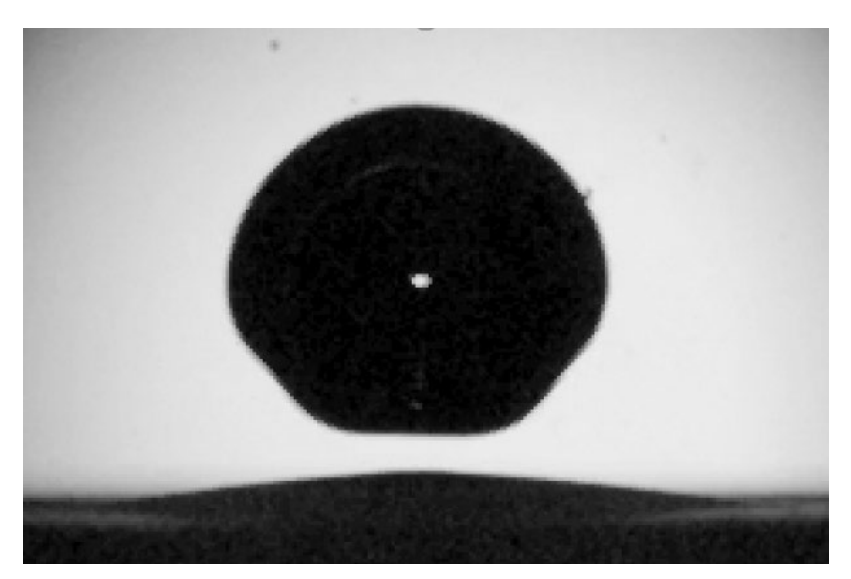
$$\overline{\sigma} = \frac{4}{3\pi} \frac{E}{(1 - \nu^2)\Delta p}$$



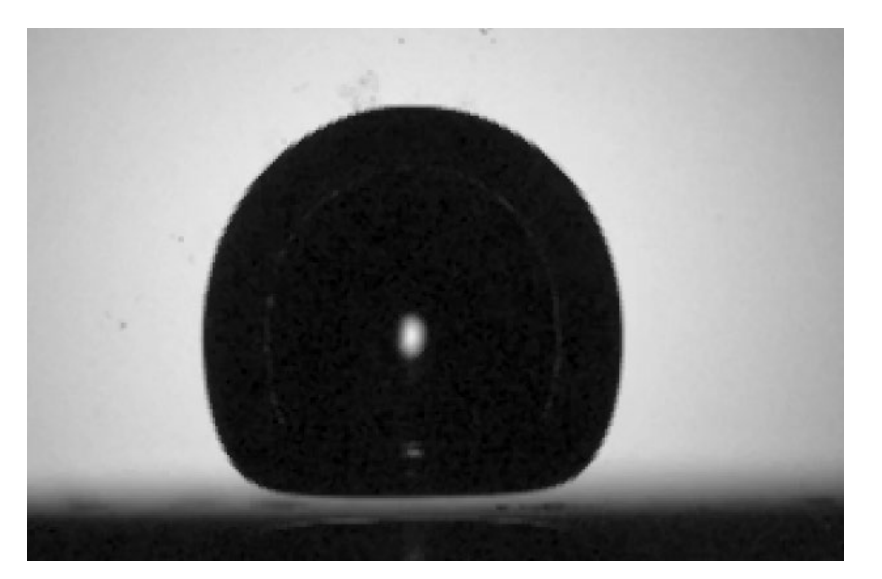
Agarose hydrogel: ρ_a , p_a and $\mathbf{u_a}$

Bubble dynamics near elastic boundary v.s. rigid boundary Bubbles at $\gamma \approx 0.8$:

- Compression and elastic rebound of the hydrogel \rightarrow different bubble dynamics.
 - Bubble shape: mushroom-like v.s. hemispherical.
 - Micro-jet precursor: side walls involution v.s. upper hemisphere involution.
 - Rebound: two sub-bubbles v.s. one single bubble.



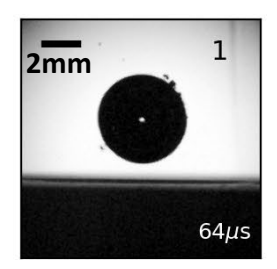
2% agarose hydrogel: $\gamma \approx 0.8, R_{max} \approx 3.7mm$, 200k fps

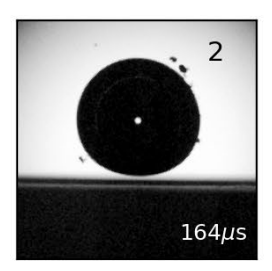


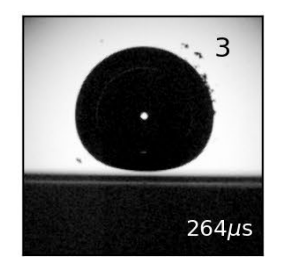
Rigid boundary: $\gamma \approx 0.8$, $R_{max} \approx 3.7mm$, 200k fps

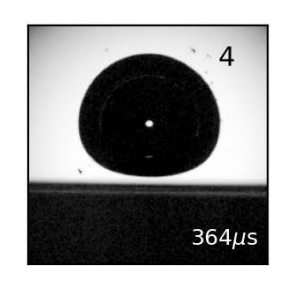
Towards mushroom-shaped bubbles

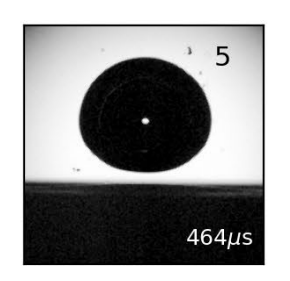
3% agarose hydrogel, $\gamma \approx 0.8$, $R_{max} \approx 3.7~mm$: experiment and simulation

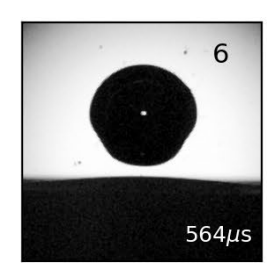


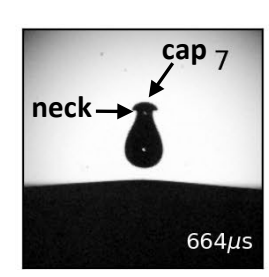


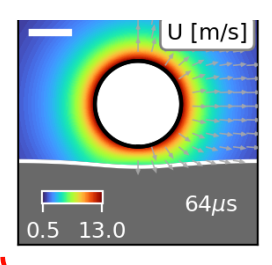


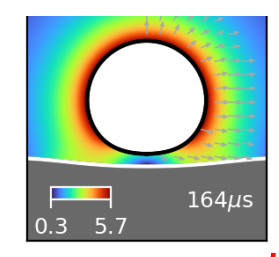


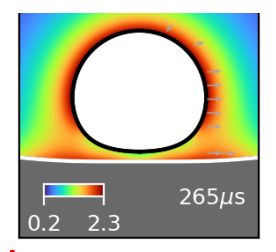


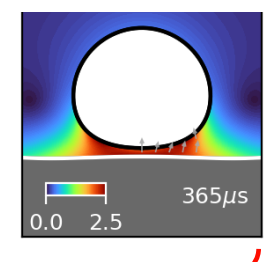


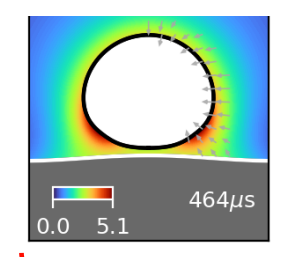


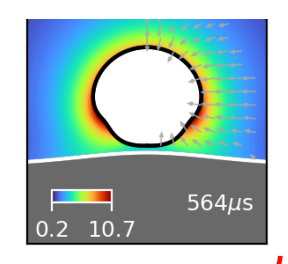




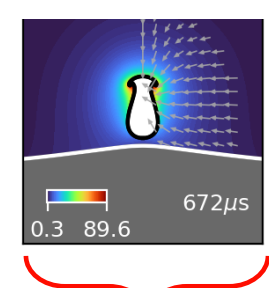








Page 35



Early bubble growth:

- Elastic boundary compressed downwards.
- Flattening of the bubble lower hemisphere.

Late bubble growth:

- Elastic boundary bounces back.
- Flattening of the bubble lower hemisphere

Bubble collapse:

- Elastic boundary forms a mound.
- Indentation of the bubble sidewalls.

Mushroom-shaped bubble:

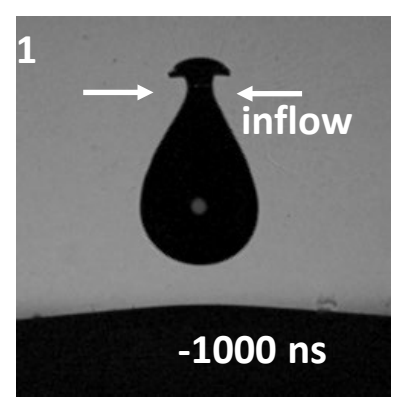
- Hemispherical cap.
- Indented neck.

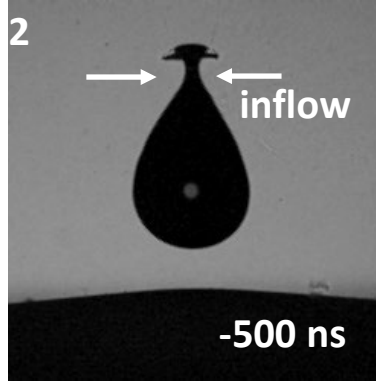


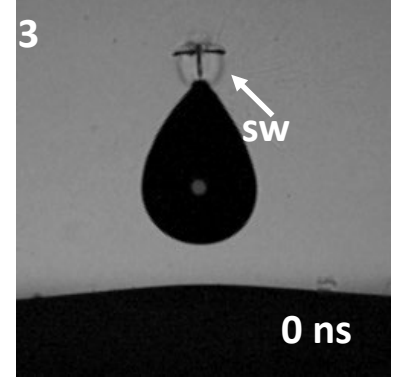
Micro-jets (1)

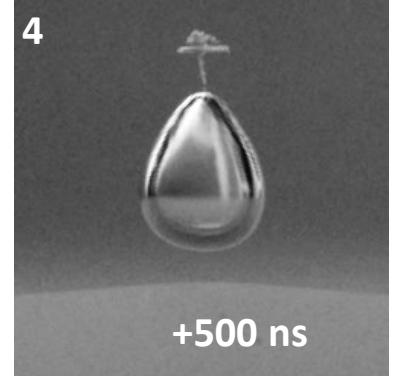
- Micro-jet initiation mechanism:
 - Annular inflow of liquid at the bubble axis of symmetry (1-2).
 - Collision of inflow produces a shockwave (3).
 - Formation of thin and very fast micro-jet forms (4-5)

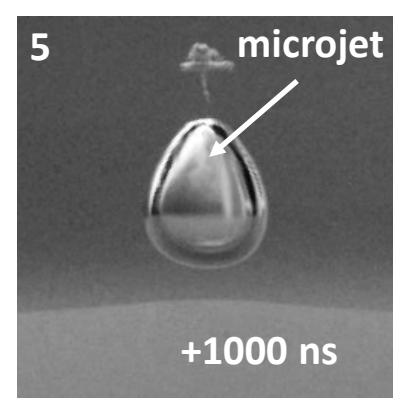
$$\Rightarrow u_{jet} \in [200 - 1000] \ m/s$$







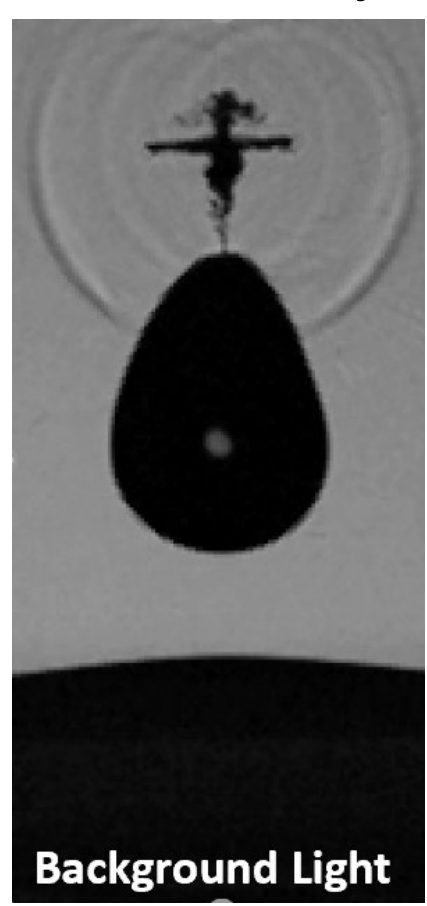


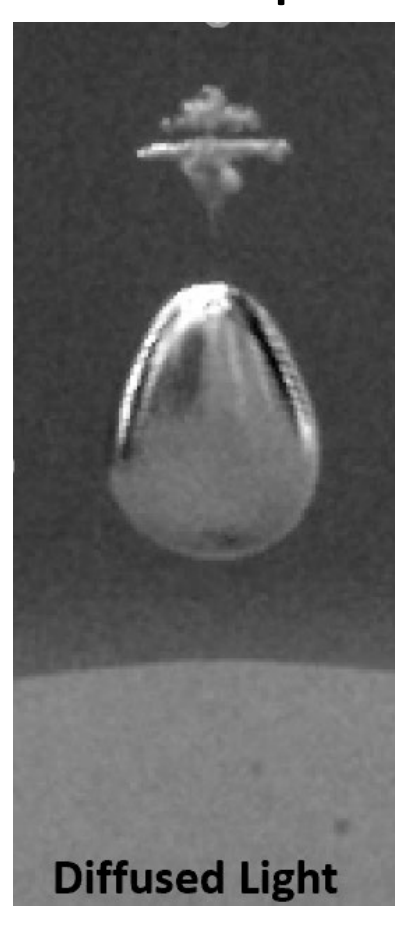


3% agarose , $\gamma\approx~0.\,8$, $R_{max}\approx~3.\,7~mm$

Micro-jets (2)

Micro-jet atomization preceding the establishment of a fully liquid micro-jet





Possible causes of jet atomization:

- Instability of the high speed micro-jet:
 - ► Liquid jet stability is characterized by Weber Nb:

Page 37

$$We = \frac{\rho_g u_{jet}^2 d}{\sigma_s}$$

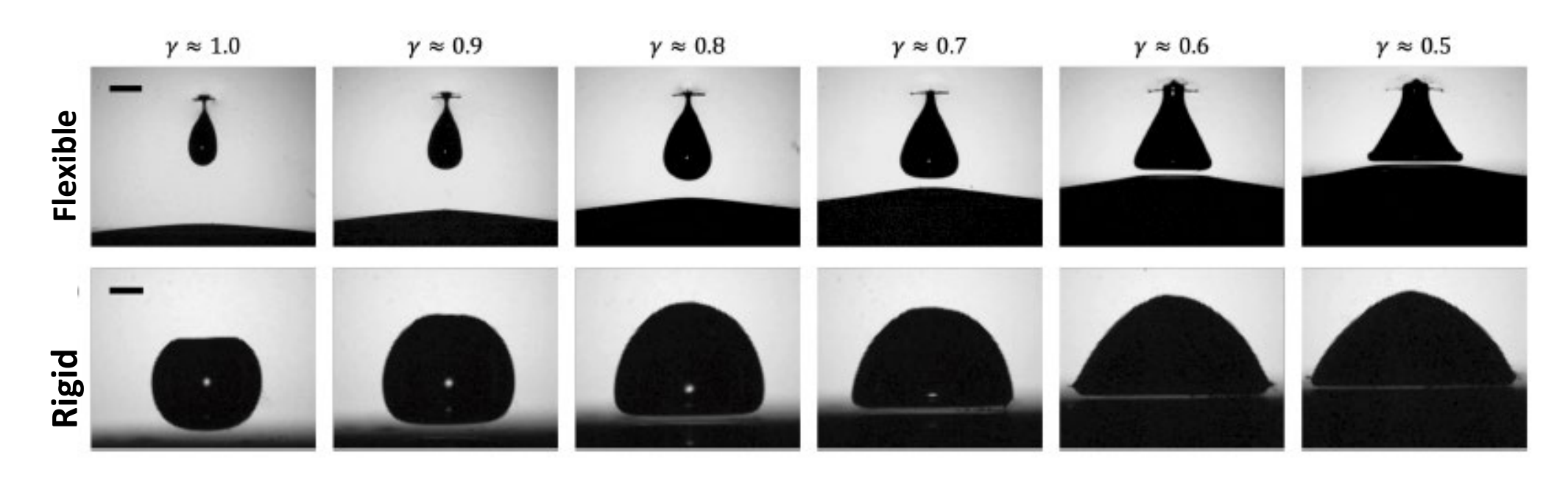
Agarose hydrogel ($\gamma = 0.8$) $\rightarrow We \approx 35$ Rigid boundary at($\gamma = 0.8$) $\rightarrow We \approx 1.1$

- Interactions with shock-waves:
 - Richtmyer–Meshkov instabilities.
- Sudden vaporization in the rarefied bubble atmosphere.

2% agarose , $\gamma \approx 0.8$, $R_{max} \approx 3.7$ mm 10 million fps

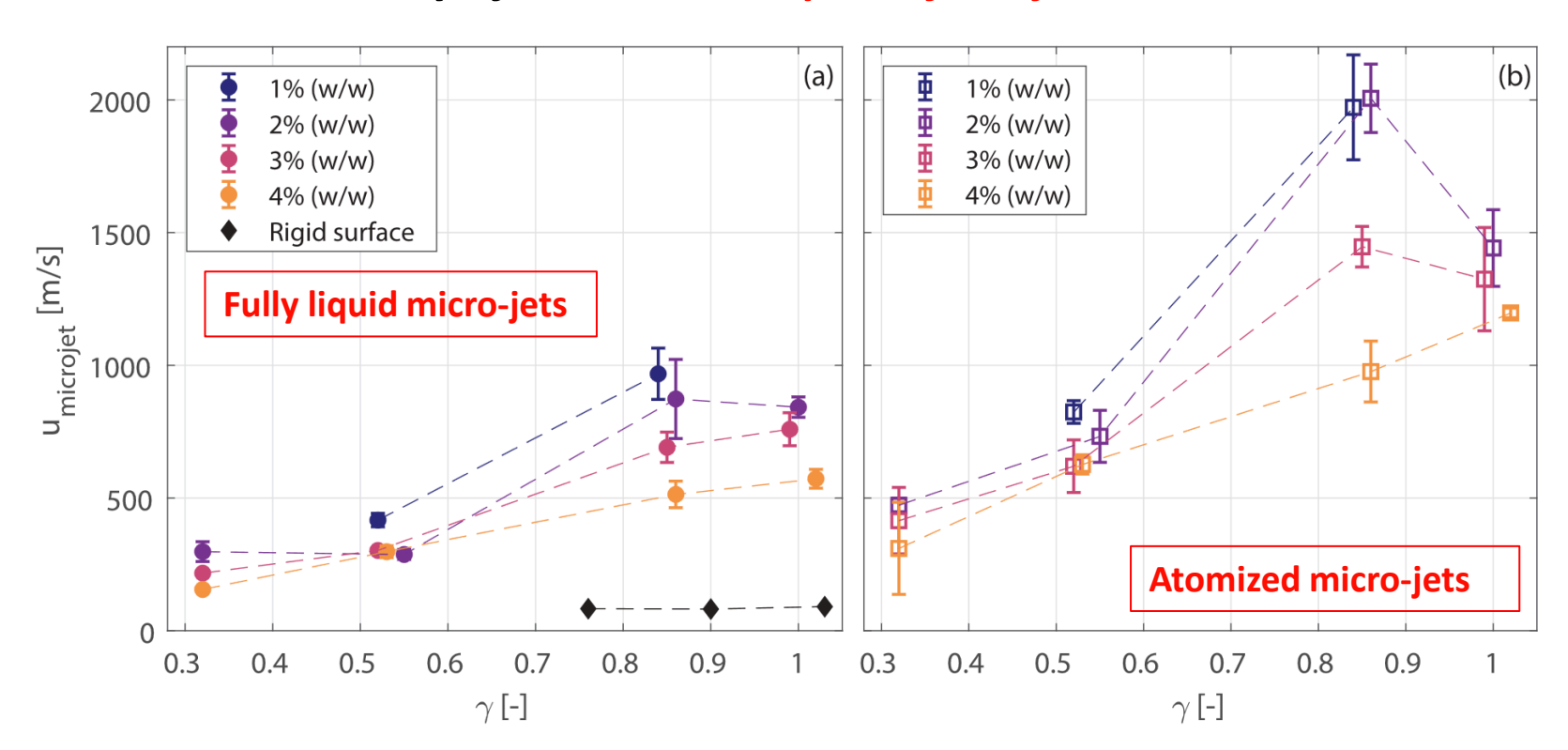
Rigid v.s. elastic boundary (effect of standoff distance):

- Snapshots of the bubble near the 2% (w/w) agarose hydrogel taken 0.2 μ s before microjet formation
- Snapshots of a similar bubble near a rigid boundary taken at the same time instant after bubble generation.



Micro-jets (3)

- Micro-jet velocities
 - Depends on both the stand-off distance and hydrogel elasticity
 - \circ Maximum velocity of the fully liquid micro-jet: \sim 1000 m/s or Ma = 2.4
 - \circ Maximum velocity of the atomized part of the jet: \sim 2000 m/s or Ma = 4.8



A. Sieber et al., Cavitation bubble dynamics & microjet atomization near tissue-mimicking materials, Phys. of Fluids, 2023.



Collapse of laser induced bubble in a flowing water

PhD Thesis, Marc Tinguely, 2013

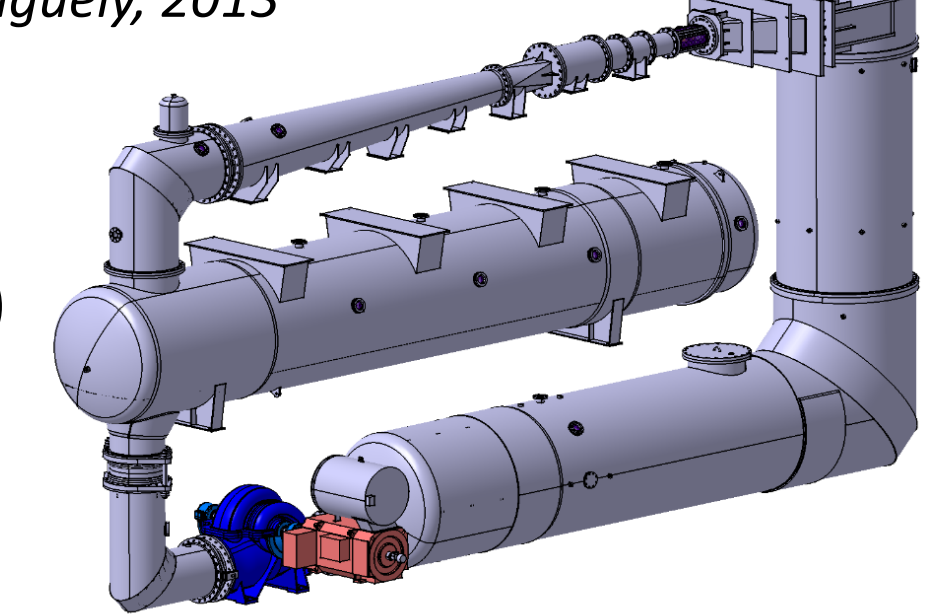


Hydrofoil : NACA 0009 truncated

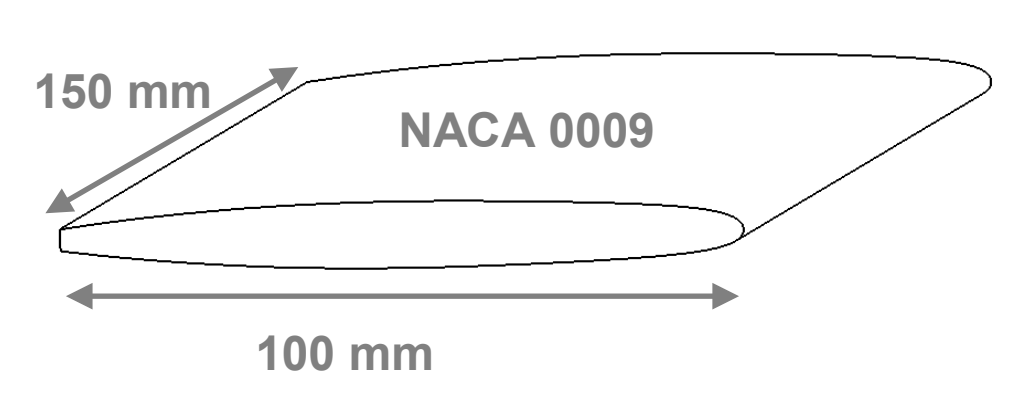
- Inlet velocity: 15 m/s ($Re = 1.5 10^6$)

- Incidence Angle : $\alpha = 1^{\circ}$

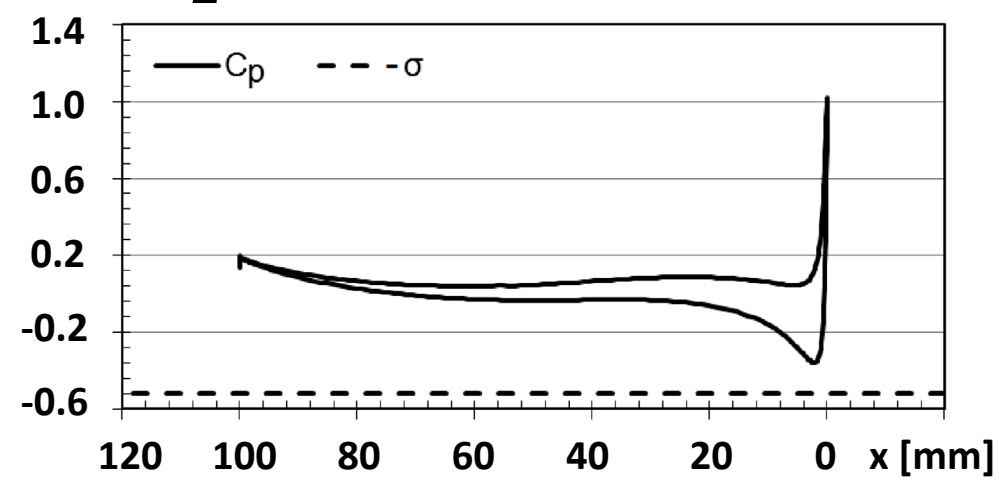
- Cavitation Coefficient : $\sigma = 0.4$



$$c_p(M) = \frac{p_M - p_{ref}}{\frac{1}{2}\rho C_{ref}^2}$$



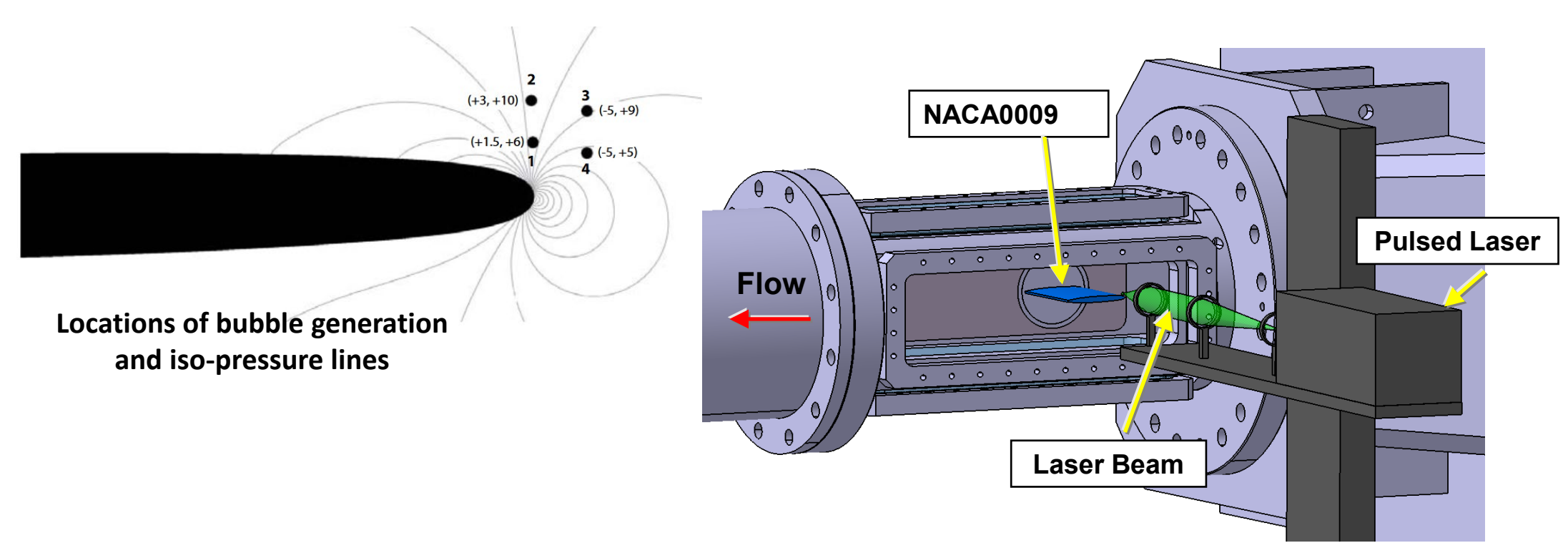
$$\sigma = \frac{p_{ref} - p_v(T)}{\frac{1}{2}\rho C_{ref}^2}$$



Collapse of laser induced bubble in a flowing water Bubble Generation

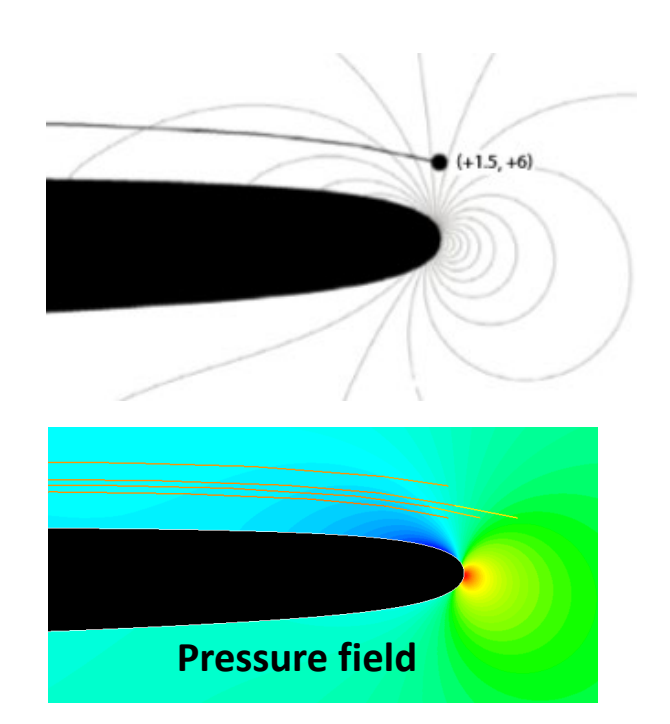
On demand bubble generation in a flowing liquid

- Pulsed Laser focused within the liquid flow
- Transparent glass window (high transmissibility for the specific wavelength of the laser)
- Possibility to create a bubble anywhere in the test section
 - → investigation of the dynamic of a single bubble in a flowing water
- Visualization with a high speed camera





Case 1: Jet towards the solid surface



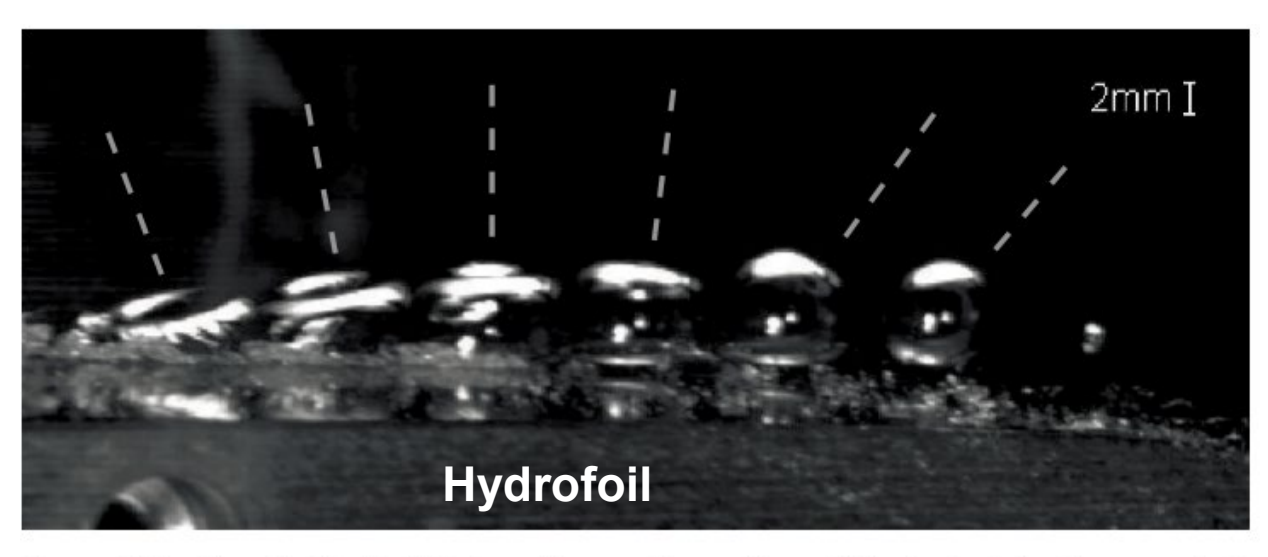
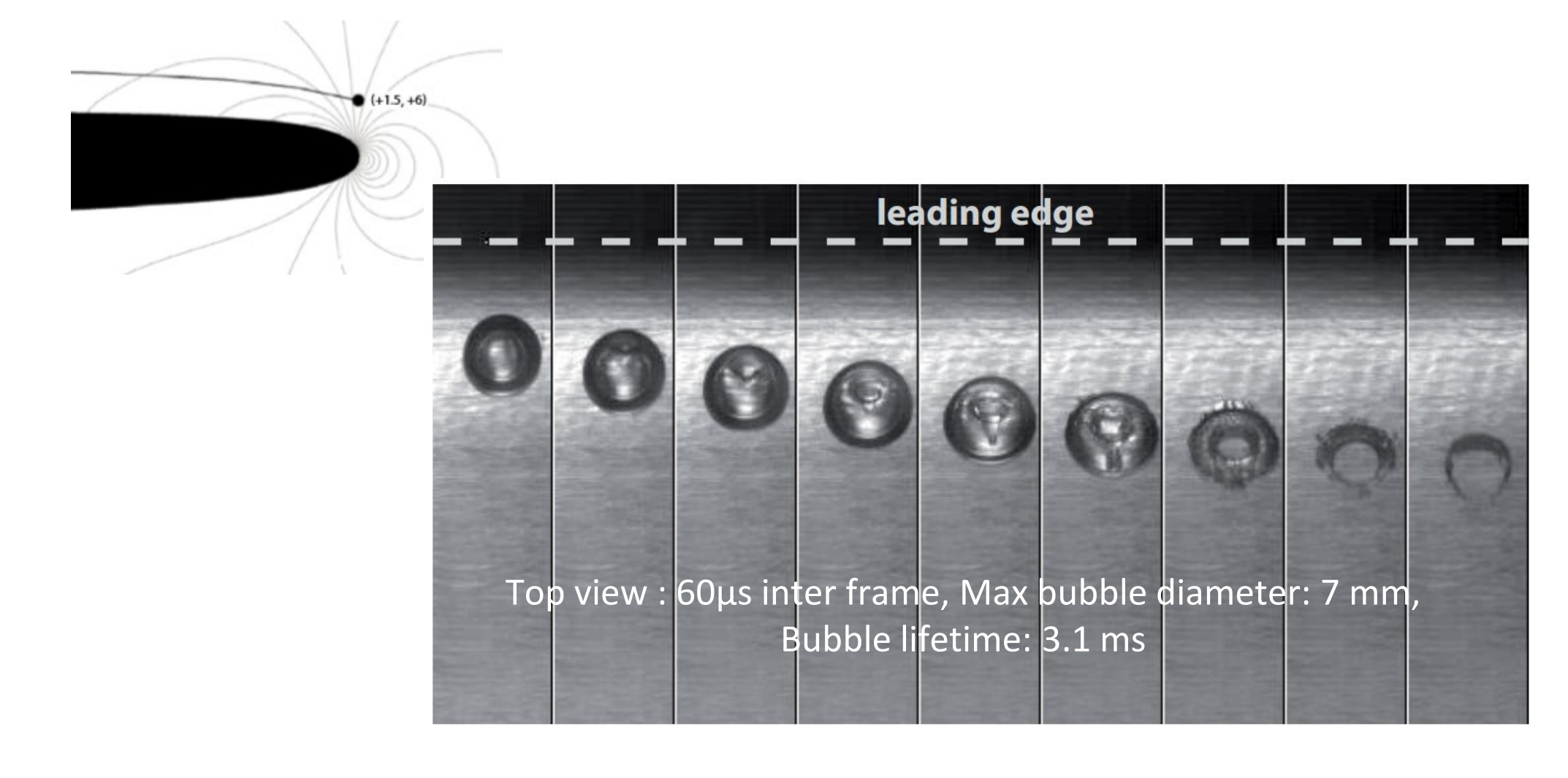


Figure 3.11: Case 1: The bubble traveling on the surface of the hydrofoil. The grey dash lines are the axis perpendicular to the flap top of the bubble and passing through the center. Interframe time: $400 \mu s$, maximum diameter: 7 mm, bubble lifetime: 3.1 ms.

Case 1: Jet towards the solid surface (top view)





Case 2: Jet towards the solid surface

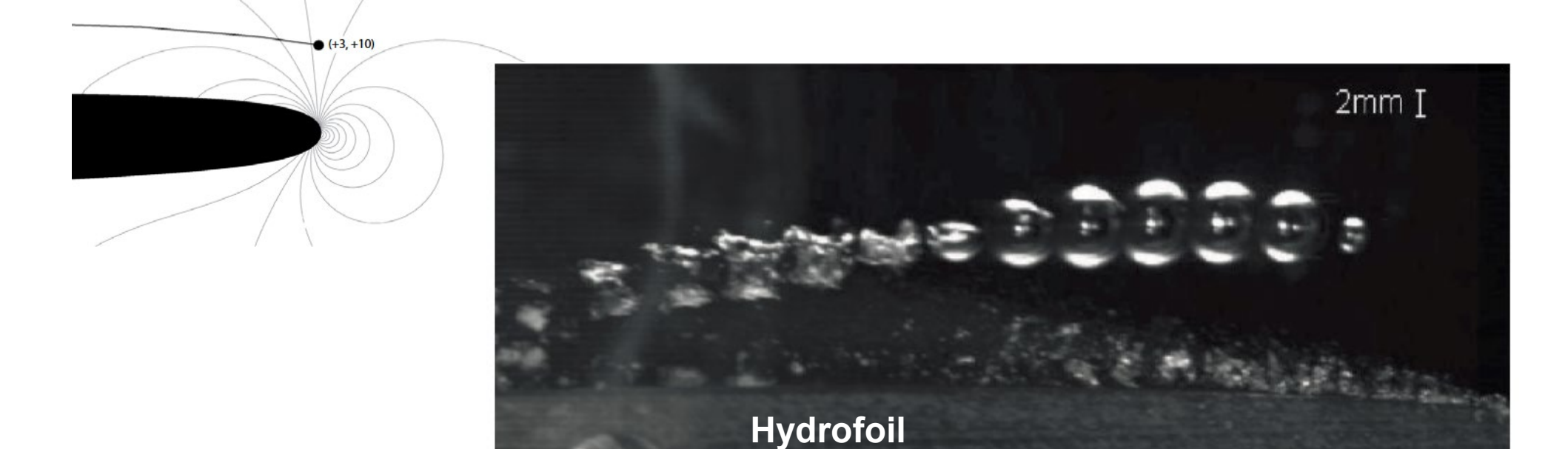


Figure 3.16: Case 2: Collapse of a bubble above the hydrofoil. The collapse is not spherical, it is initiated at the top of the bubble. Interframe time: 200 μ s, maximum diameter: 7 mm, bubble lifetime: 1.28 ms.

Case 3: Jet towards the pressure gradient

(-5, +9)

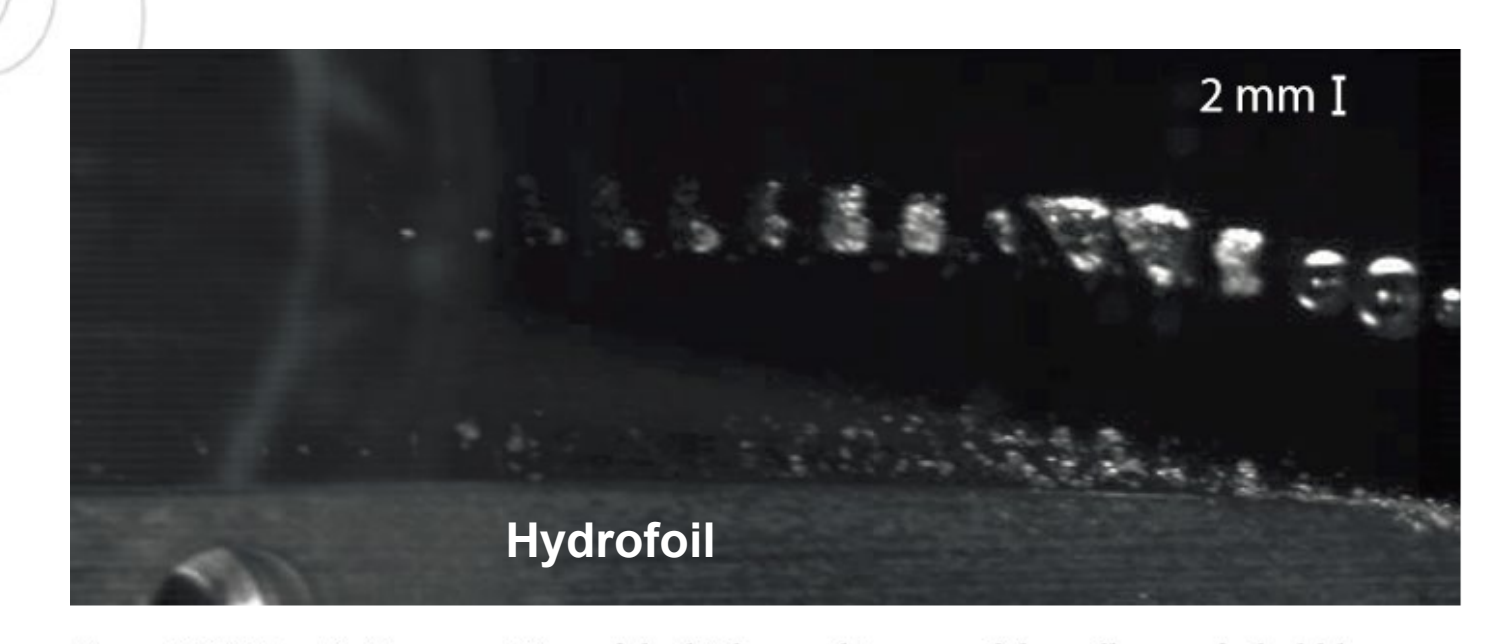
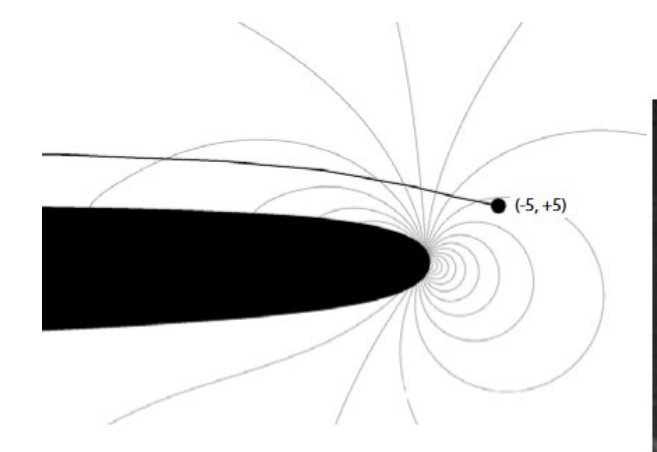


Figure 3.18: Case 3: Superposition of the high speed images of the collapse of a bubble generated at (-5, +9). The bubble bubble has a microjet not towards the solid surface. Interframe time: 180 μ s, maximum diameter: 5 mm, bubble lifetime: 440 μ s.



Case 4:

- 1st collapse Jet towards the pressure gradient
- 2nd collapse towards the solid surface



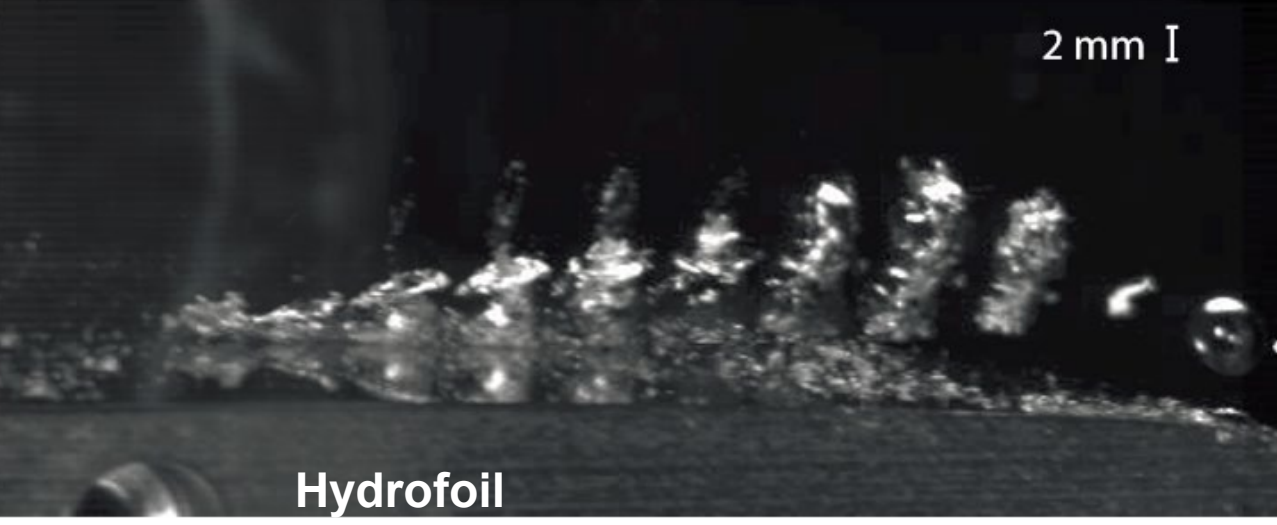


Figure 3.22: Case 4 : Superposition of the high speed images of the collapse of a bubble generated at (-5, +5). The bubble collapses upstream to the leading edge. The rebound, a cloud of microbubbles, travels and collapses on the surface of the hydrofoil. Interframe time: $200 \ \mu s$. Initial bubble maximum diameter: $5 \ mm$, lifetime: $380 \ \mu s$. Rebound bubble maximum diameter: $6 \ mm$, lifetime: $2 \ ms$.

Collapse of laser induced bubble in a flowing water Dynamics of rebound cavity

Rebound cavity is made of a cluster of microbubbles

- The cluster of microbubbles behaves as a single bubble
- Micro jet towards the solid surface
- → Rebound bubble may be more aggressive than the original bubble!

